Developmental Biology 455 (2019) 434–448

Contents lists available at ScienceDirect

Developmental Biology

journal homepage: www.elsevier.com/locate/developmentalbiology

Molecular patterning of the embryonic cranial mesenchyme revealed by genome-wide transcriptional profiling

Krishnakali Dasgupta, Jong Uk Chung, Kesava Asam, Juhee Jeong *

Department of Basic Science and Craniofacial Biology, New York University College of Dentistry, New York, NY, 10010, USA

ARTICLE INFO

Keywords:
Transcriptional profiling
Meninges
Calvaria
Cranial mesenchyme
Craniofacial development
Mouse

ABSTRACT

In the head of an embryo, a layer of mesenchyme surrounds the brain underneath the surface ectoderm. This cranial mesenchyme gives rise to the meninges, the calvaria (top part of the skull), and the dermis of the scalp. Abnormal development of these structures, especially the meninges and the calvaria, is linked to significant congenital defects in humans. It has been known that different areas of the cranial mesenchyme have different fates. For example, the calvarial bone develops from the cranial mesenchyme on the baso-lateral side of the head just above the eye (supraorbital mesenchyme, SOM), but not from the mesenchyme apical to SOM (early migrating mesenchyme, EMM). However, the molecular basis of this difference is not fully understood. To answer this question, we compared the transcriptomes of EMM and SOM using high-throughput sequencing (RNA-seq). This experiment identified a large number of genes that were differentially expressed in EMM and SOM, and gene ontology analyses found very different terms enriched in each region. We verified the expression of about 40 genes in the head by RNA in situ hybridization, and the expression patterns were annotated to make a map of molecular markers for 6 subdivisions of the cranial mesenchyme. Our data also provided insights into potential novel regulators of cranial mesenchyme development, including several axon guidance pathways, lectin complement pathway, cyclic-adenosine monophosphate (cAMP) signaling pathway, and ZIC family transcription factors. Together, information in this paper will serve as a unique resource to guide future research on cranial mesenchyme development.

1. Introduction

During embryogenesis, the brain forms from the rostral part of the neural tube after gastrulation. As the neural tube closes, the brain becomes covered with a sheath of mesenchyme cells from the neural crest and the mesoderm. This cranial mesenchyme (also known as prima meninx) will develop into three types of tissues surrounding the brain, namely, the meninges, the calvaria (top part of the skull), and the dermis of the scalp, in the inside to outside order (Angelov and Vasilev, 1989; Dasgupta and Jeong, 2019; O'Rahilly and Muller, 1986). The mature meninges consist of the pia mater, the arachnoid mater, and the dura mater. The calvaria at birth is a composite of plates of bone and the soft tissue joints called sutures. Cartilage also appears during early development the calvaria, but it is subsequently degraded as the bone grows over it (Ferguson and Atit, 2019). Abnormal development of the meninges or the calvaria underlies several human congenital defects, including Dandy-Walker malformation (hypoplasia of the cerebellum, which can be caused by meningeal deficiency) and craniosynostosis (premature fusion of the suture(s)) (Aldinger et al., 2009; Siegenthaler and Pleasure, 2011; Twigg and Wilkie, 2015). Insights into these conditions can be obtained from knowledge of the molecular genetic mechanisms regulating cranial mesenchyme development.

How the wide array of tissues differentiate from the cranial mesenchyme is poorly understood. Previous studies in mice have shown evidence of patterning along two different axes of the cranial mesenchyme by embryonic day (E) ~12.5 (mouse gestation is 19 days). At this stage, the rudiments for the frontal bone and the parietal bone of the calvaria emerge in the basolateral cranial mesenchyme just above the eye, termed the supraorbital ridge or the supraorbital mesenchyme (SOM) (Deckelbaum et al., 2012; Ferguson and Atit, 2019; Ishii et al., 2015). Here, the dermis develops just outside the osteogenic layer while the cartilage forms just inside the osteogenic layer. The canonical WNT (wingless/int) signaling and TWIST transcription factors have been shown to regulate the specification of the progenitors for the dermis and the calvarial bone, by preventing them from adopting the chondrogenic fate like the cells located further inside (Day et al., 2005; Goodnough et al., 2012; Tran

* Corresponding author.
E-mail address: jj78@nyu.edu (J. Jeong).

https://doi.org/10.1016/j.ydbio.2019.07.015
Received 25 March 2019; Received in revised form 22 July 2019; Accepted 22 July 2019
Available online 24 July 2019

et al., 2010).

The mesenchyme lying apical to SOM at E12-E13, termed the early migrating mesenchyme (EMM), does not generate ossification centers (Roybal et al., 2010). This difference between EMM and SOM suggests that the apical-basal patterning of the cranial mesenchyme has spatially restricted the osteogenic potential of the cells. In addition, the apical-basal patterning most likely plays an important role in subsequent growth of the calvarial bone. After the initiation of osteogenesis in SOM, the frontal bone and the parietal bone grow toward the apex over several days before birth. Cell tracing studies have shown that this apical expansion is driven by migration of the cells from SOM, rather than by the recruitment of EMM cells that are present on the apical side prior to the osteogenic front (Roybal et al., 2010; Yoshida et al., 2008). The basal-to-apical migration of SOM cells raises a question whether there are molecular cues along this axis to guide the cells.

To better understand the apical-basal patterning of the cranial mesenchyme, it is essential to have comprehensive information on region-specific gene expression. In this study, we compared the transcriptomes of EMM and SOM of mouse embryos during normal development. A large number of differentially expressed genes were identified, and gene ontology (GO) analyses revealed distinct categories associated with each region. Furthermore, we examined and annotated the expression of ~40 genes by RNA in situ hybridization on head sections, generating a unique resource on the molecular patterning of the embryonic cranial mesenchyme.

2. Results

2.1. Transcriptional profiling identifies genes that are differentially expressed between EMM and SOM during normal development

To characterize the molecular genetic differences between EMM and SOM, we conducted transcriptional profiling using high-throughput sequencing (RNA-seq). EMM and SOM were dissected from E12.5 wild type mouse embryos (Fig. 1A), and RNA-seq was performed on quadruplicate samples. E12.5 was chosen because at this stage the calvarial bone rudiments have just formed in SOM but have yet to undergo apical growth. By using the intermediate time point, we hoped to detect gene expression differences between SOM and EMM that underlie both the initial localization of the ossification centers and the subsequent directional migration of the osteogenic cells.

A principal component analysis of the transcriptomes of all 8 samples showed a stark difference between EMM and SOM, as well as strong correlations among the replicates within each group (Fig. 1B). To identify genes that are differentially expressed, we applied stringent criteria of $p < 0.001$ and base mean count (mean of normalized read counts from all 8 samples) > 50, to exclude genes with very low overall expression. For the fold change (FC) > 2, we obtained 1095 genes with higher expression in EMM than in SOM (= EMM^{High} genes) and 398 genes with higher expression in SOM than in EMM (= SOM^{High} genes). Because these numbers were still large, we focused on top 200 EMM^{High} genes and top

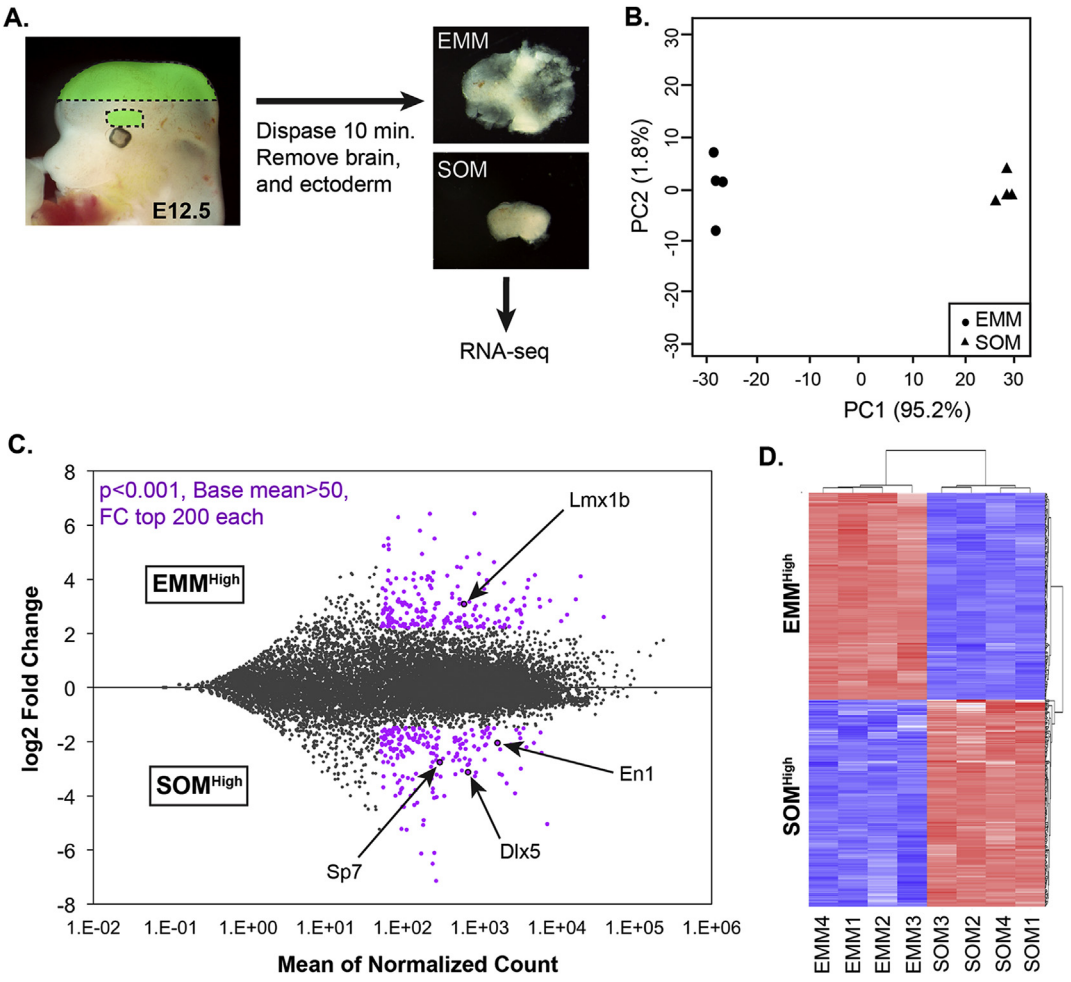

Fig. 1. Genome-wide comparison of gene expression between early migrating mesenchyme (EMM) and supraorbital mesenchyme (SOM). A) Overview of the transcriptional profiling experiment. The green color marks the areas dissected for the experiment. B) Principal component (PC) analysis of the transcriptomes of 4 EMM samples and 4 SOM samples. C) MA plot of RNA-seq result. Genes already known to be specific to EMM or SOM are indicated by arrows. D) Heatmap of RNAseq data for top 400 region-specific genes (purple dots in C).

200 SOM^{High} genes based on FC (purple in Fig. 1C, Tables S1 and S2). These sets included genes that were known to be specific to EMM (*Lmx1b*) or SOM (*En1, Dlx5, Sp7*) (Cesario et al., 2018; Deckelbaum et al., 2006; Han et al., 2007). Note that *Runx2* was not identified to be SOM^{High} here because the two isoforms of *Runx2* were counted together in RNA-seq, where only one of them is specific to the osteogenic mesenchyme (Lee et al., 2005). The heatmap for the 400 genes confirmed that their expression pattern was highly consistent across replicates (Fig. 1D).

2.2. GO analyses reveals that very different categories of genes are enriched in EMM and SOM

To assess overall molecular and cellular characteristics of EMM and SOM, we performed GO analyses on the result from RNAseq. Because various GO programs have own strengths and weaknesses, we used three programs and combined their outputs to prioritize subsequent experiments.

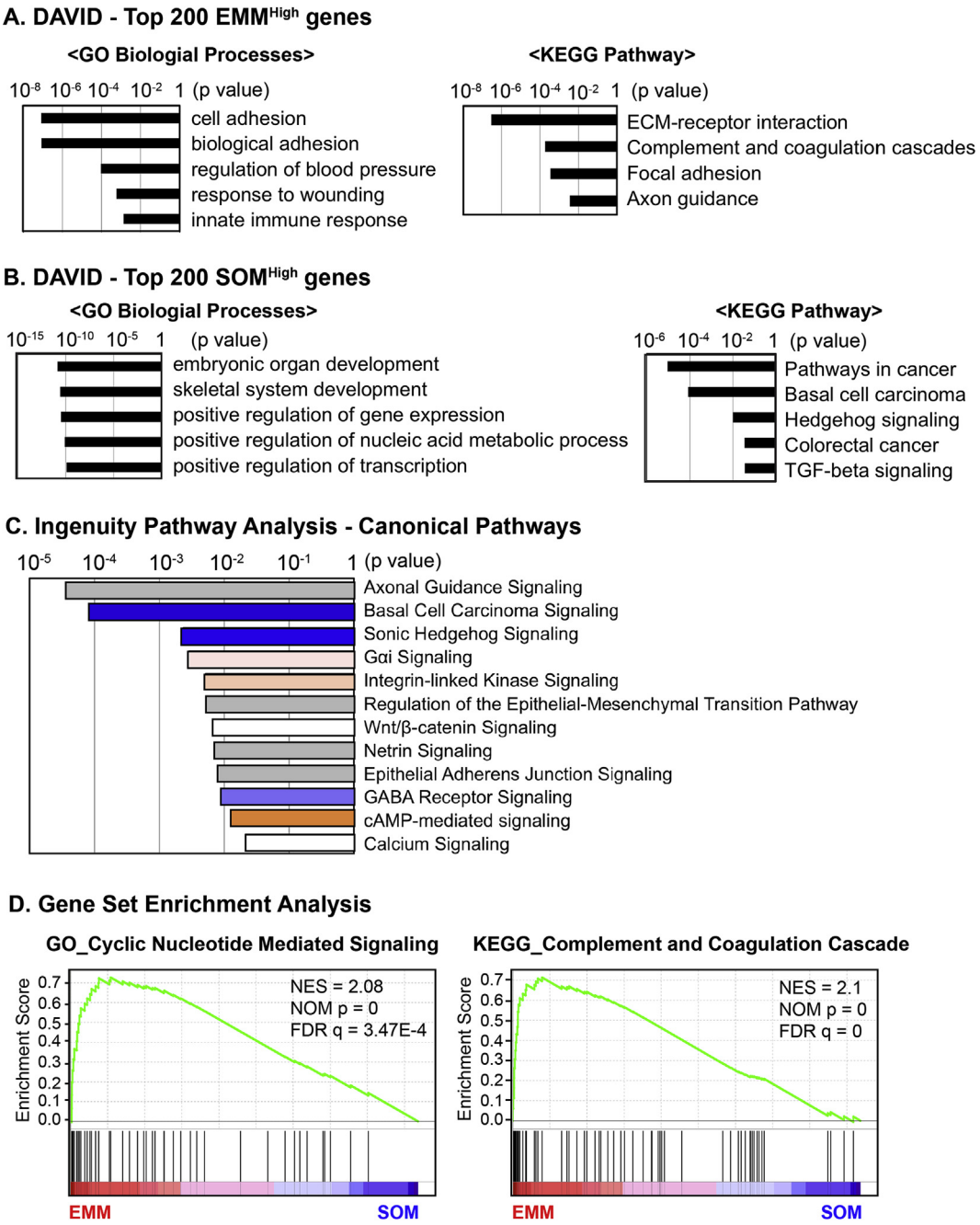

Fig. 2. Gene ontology (GO) analysis of RNA-seq result. A,B) Top 200 EMM^{High} genes and top 200 SOM^{High} genes were analyzed separately using Database for Annotation, Visualization and Integrated Discovery (DAVID). For GO Biological Processes, only top 5 most enriched terms for each gene set are shown. For KEGG Pathway, all the pathways that are significantly enriched ($p < 0.05$) are shown. Further details, including the list of genes belonging to each category, are in Tables S3 and S4. C) Canonical pathways identified by Ingenuity Pathway Analysis (IPA) to be associated with top 400 region-specific genes. Out of 31 canonical pathways that showed significant association (Table S5), 12 pathways most relevant to development are listed. The colors indicate relative activities of the pathway in EMM and SOM based on computational predictions by IPA. Blue: higher activity in SOM than in EMM, orange: higher activity in EMM than in SOM, white: no difference in activity between EMM and SOM, gray: unable to make a prediction. For blue and orange, the intensities of the colors reflect the z scores for the difference. D) Enrichment plots for select categories associated with EMM from Gene Set Enrichment Analysis (GSEA). Additional results from GSEA are in Tables S6 and S7. NES: normalized enrichment score, NOM p: normalized p value, FDR q: false discovery rate q value.

First, we used the Database for Annotation, Visualization and Integrated Discovery (DAVID) (Huang et al., 2009) to identify GO terms associated with top 200 EMM^{High} genes and top 200 SOM^{High} genes separately (Tables S3 and S4). Top Biological Processes (BP) terms for EMM^{High} genes were mostly related to cell adhesion, blood and immune responses, and cell surface signaling (Fig. 2A; Fig. S1). Top BP terms for SOM^{High} included 'skeletal system development', which was consistent with SOM being the source of the calvarial bone and the transient cartilage. The other terms were mainly related to gene expression (Fig. 2B; Fig. S2). EMM^{High} genes and SOM^{High} genes were also associated with distinct pathways annotated by Kyoto Encyclopedia of Genes and Genomes (KEGG). For EMM^{High} genes, 'axon guidance' and 'complement and coagulation cascade' were notable (Fig. 2A). SOM^{High} genes were associated with pathways involved in cancer, many of which also regulate development (Fig. 2B).

Second, we performed Ingenuity Pathway Analysis (IPA), with an input of a combined gene set of top 200 EMM^{High} genes and top 200 SOM^{High} genes (= top 400 region-specific genes). IPA can discern different patterns of gene expression (EMM^{High} vs. SOM^{High}) within the gene set, and use this information to predict relative activities of a given pathway between the two regions. Components of 31 IPA canonical pathways were over-represented in the top 400 region-specific genes (Table S5), and 12 pathways most relevant to development are listed in Fig. 2C. There was a considerable overlap between the pathways identified by IPA and by DAVID. Interestingly, 'axon guidance signaling' was one of the most significantly over-represented pathways according to IPA. When the predicted activities were compared, 'basal cell carcinoma signaling' and 'Sonic hedgehog signaling' showed the most SOM-specific activities, while 'cAMP-mediated signaling' showed the most EMM-specific activity (Fig. 2C).

Third, we performed Gene Set Enrichment Analysis (GSEA) (Subramanian et al., 2005). The input for this program was the expression data for the whole genome (23,418 genes) from each of the 8 samples. Table S6 lists 10 GO BP terms and 10 KEGG pathways that are most significantly associated with EMM. Several categories were repeated from the other programs, including 'cyclic-nucleotide mediated signaling' and 'complement and coagulation cascade' (Fig. 2D). The top categories associated with SOM were mainly related to ribosomes and nucleic acid (Table S7), which was reminiscent of DAVID GO BP result for SOM^{High} genes (Fig. 2B).

2.3. Validation of RNA-seq results and annotation of gene expression in the cranial mesenchyme

We combined the above in silico results with information in the literature to choose 7 categories of genes that are likely to be important for patterning of the cranial mesenchyme (listed below). We then verified the expression of select genes from each category using reverse transcription followed by quantitative real-time PCR (RT-qPCR) and/or RNA in situ hybridization on sections of the head. We placed more emphasis on EMM^{High} genes because far less is known about development of EMM than SOM. Total 45 genes from the top 400 region-specific genes were examined by RT-qPCR (33 EMM^{High} and 12 SOM^{High}), using EMM and SOM dissected from E12.5 wild type embryos. 35 of them showed the differential expression consistent with RNA-seq (25 EMM^{High} and 10 SOM^{High}) (Figs. S3 and S4; results are also indicated in the main figures below). We performed section RNA in situ hybridization for ~100 genes out of the top 400 region-specific genes, and the results for 36 genes are described below. RNA in situ hybridization produced no detectable signal for many of the genes tested, reflecting the limited sensitivity of the conventional method.

To annotate the results from RNA in situ hybridization, we defined the subdomains of the cranial mesenchyme at E12.5 (Fig. S5). The laminin-rich basement membrane forms the boundaries between the mesenchyme and the surface ectoderm, and between the mesenchyme and the brain. We also used *Prrx1-Cre*, which is specific to the mesenchyme, to label the cranial mesenchyme with yellow fluorescence protein (YFP) from a Cre reporter (Figs. S5C–J,R–Y) (Logan et al., 2002; Soriano, 1999; Srinivas et al., 2001). EMM can be divided into two layers based on the organization of the cells, the dense outer layer and the reticular inner layer (Angelov and Vasilev, 1989; Dasgupta and Jeong, 2019) (Figs. S5A–K,P-Z). The inner layer is considered the 'meningeal layer' (Angelov and Vasilev, 1989), and it has many blood vessels that are also surrounded by the laminin-rich basement membrane (Fig. S5H,W). SOM can be divided into four layers, namely, the outermost dermal layer, the osteogenic layer (expressing *Runx2*), the chondrogenic layer (expressing *Sox9*), and the meningeal layer (internal to the chondrogenic layer) (Fig. S5L-O,a-d). The same 6 subdomains can be defined in the sections through the frontal bone rudiment (Fig. S5A-O) and through the parietal bone rudiment (Fig. S5P-d).

We first annotated the expression of 5 transcription factor genes known to be important regulators of cranial mesenchyme patterning. Each had a distinct pattern of expression, including some details that had not been noted previously (Fig. S6; Table 1). *Msx1* (Msh homeobox 1) and *Msx2* (Msh homeobox 2) have overlapping roles in calvarial development, promoting osteogenesis in SOM while suppressing it in EMM (Han et al., 2007; Roybal et al., 2010; Wilkie et al., 2000). Both genes were strongly expressed in the outer EMM and the osteogenic SOM (Fig. S6A-L). However, only *Msx1* was significantly expressed in the meningeal layer (Figs. S6B,C,E,F). *Twist1* (twist basic helix-loop-helix transcription factor 1) is known to regulate the patterning of SOM (see Introduction). It was also highly expressed in the outer EMM (Figs. S6M–R). *Lmx1b* (LIM homeobox transcription factor 1 beta) is expressed specifically in EMM and inhibits calvarial osteogenesis (Cesario et al., 2018). It was mainly in the outer EMM and less in the meningeal EMM (Figs. S6S–V). *En1* (engrailed 1) is the earliest marker of SOM, being detected here from ~E11 (Deckelbaum et al., 2006). *En1* expression was mostly in the osteogenic SOM at E12.5 (Fig. S6W-Z).

We used this annotation system for all the RNA in situ hybridization data in the current paper, and summarized the results in Table 1. In addition, many of the genes examined here had significant expression in the brain, and thus brief descriptions of the expression patterns in the brain (telencephalon and diencephalon) are also provided.

2.3.1. Skeletal development

While many genes in this category had already been examined by others (Fig. 3A), expression of *Eya1* (EYA transcriptional coactivator and phosphatase 1) had not been described in the cranial mesenchyme despite the report of calvarial bone deficiency in mouse *Eya1* mutants (Xu et al., 1999). We found that *Eya1* was expressed in the osteogenic SOM and the chondrogenic SOM at E12.5, but subsequently down-regulated in the bone rudiments by E13.5 (Fig. 3B–I; Figs. S7A–C). *Eya1* was also detected in the brain, specifically, in the developing hippocampus of the telencephalon (Fig. 3E). SOX6 is one of the key transcription factors for cartilage development (Akiyama and Lefebvre, 2011), but more recently it was detected in the developing bones of the face that do not go through a cartilage intermediate (Watanabe et al., 2016). Furthermore, a disruption in human *SOX6* was reported in a craniosynostosis patient (Tagariello et al., 2006), which suggested that SOX6 might be involved in calvarial development. Both osteogenic SOM and chondrogenic SOM expressed *Sox6* at E12.5, and unlike *Eya1*, *Sox6* expression continued in both subdivisions at E13.5 (Fig. 3J-N; Figs. S7D–F). In the brain, *Sox6* was broadly expressed in the cortex and in the pallidum of the basal ganglia (Fig. 3J).

2.3.2. Cancer pathways

Genes in this category included members of Hedgehog, WNT, BMP (bone morphogenetic protein), and FGF (fibroblast growth factor) pathways (Fig. 4A). We focused on the canonical WNT pathway because it is involved in development of the cranial mesenchyme on the apical side as well as the baso-lateral side (Choe et al., 2014; DiNuoscio and Atit, 2019; Ferguson and Atit, 2019). *Frzb* (frizzled-related protein) encodes an

Table 1
Summary of gene expression in the cranial mesenchyme at E12.5

Gene	Frontal bone level						Parietal bone level					
	EMM		SOM				EMM		SOM			
	Menin.	Outer	Menin.	Chond.	Osteo.	Derm.	Menin.	Outer	Menin.	Chond.	Osteo.	Derm.
Msx1	+++	+++	+++	++	+++	–	+++	+++	+++	++	+++	–
Msx2	+	+++	–	+	+++	–	+	+++	–	+	+++	–
Twist1	+	+++	+	–	++	+++	+	+++	+	–	++	+++
Lmx1b	+	+++	–	–	–	–	+	+++	–	–	–	–
En1	–	–	–	–	+++	–	–	–	+	–	+++	–
Eya1	–	–	–	++	+	–	–	–	–	+	++	–
Sox6	–	–	–	++	++	–	–	–	–	++	++	–
Frzb	+	–	–	–	–	–	–	–	–	–	–	–
Myc	–	–	–	++	++	++	–	–	–	++	++	++
Sox11	–	–	–	+	+	++	–	–	–	+	+	++
Lef1	–	–	–	–	++	+++	–	–	+	–	++	+++
Fzd9	–	–	–	+	–	–	–	–	–	+	–	–
Rspo3	–	–	–	–	++	++	–	–	–	–	++	
Axin2	++	++	+	–	++	+++	++	++	+	–	+	+++
Lamc3	+++	–	+++	–	–	–	+++	–	+++	–	–	–
Lama1	+++	–	+++	–	–	–	+++	–	+++	–	–	–
Sned1	+++	–	+++	–	–	–	+++	–	+++	–	–	–
Sorbs1	+++	+++	++	++	–	–	+++	+++	++	+++	–	–
Pcdh7	+	+	–	–	++	+	+	++	–	–	+	++
Wisp1	+	+++	+	–	+	+	+	+++	+	–	+	+
Sema3c	+	+++	–	–	–	–	+	+++	–	–	–	–
Nrtk2	++	–	++	–	–	–	++	–	++	–	–	–
Epha7	++	++	++	–	–	+	++	++	++	–	–	+
Ephb3	–	–	–	++	++	+++	–	–	–	+	++	++
Unc5b	–	–	–	–	++	+	–	–	–	–	+	+
Unc5c	+	+	+	++	–	+	+	+	+	++	–	–
Dcc	–	–	–	–	–	+	–	–	–	–	–	+
Gng4	–	–	–	–	–	+	–	–	–	–	–	+
Colec12	++	++	+	–	–	–	++	++	+	–	–	++
Masp1	+	++	–	–	–	–	+	++	–	–	–	++
Calca	+	+	++	–	–	–	–	–	++	–	–	–
Adra2a	++	–	++	–	–	+	++	–	++	–	–	+
Akap12	+++	+++	+++	–	–	+	+++	+++	+++	–	–	+++
Npr3	+	+	+	–	–	–	+	+	–	–	–	++
Zic1	++	++	++	–	–	–	++	++	++	–	–	++
Zic3	++	++	++	–	–	–	++	++	++	–	–	+
Zic4	+	+	–	–	–	–	+	++	–	–	–	–

The expression levels were assessed by visual inspection of RNA in situ hybridization results, and thus the table is for a quick reference only.

extracellular antagonist of WNT signaling, and it was specifically expressed in the meningeal EMM (Fig. 4D and E). *Myc* (myelocytomatosis oncogene) transcription factor gene is a downstream target of WNT signaling, and *Sox11* (SRY-box 11) encodes a transcription factor that amplifies WNT signaling (Bhattaram et al., 2014; Myant and Sansom, 2011). They were broadly expressed in SOM except for the meningeal SOM (Fig. 4F–I, Figs. S8A–D). *Sox11* was also strongly expressed in the entire brain (Fig. 4H). *Lef1* (lymphoid enhancer binding factor 1) encodes a transcriptional effector of the canonical WNT pathway (Novak and Dedhar, 1999), and it is also a transcriptional target of this pathway (Filali et al., 2002). *Lef1* was intensely expressed in the dermal SOM and moderately in the osteogenic SOM but undetectable in EMM (Fig. 4J and K; Figs. S8E and F). *Fzd9* (frizzled class receptor 9), encoding a receptor for WNT, was expressed in the chondrogenic SOM, while *Rspo3* (R-spondin 3), encoding a secreted co-activator of WNT, was expressed in the osteogenic SOM and the dermal SOM (Fig. 4L–Q; Figs. S8G–J). In the brain, *Fzd9* and *Rspo3* were expressed mostly in the dorsal part, i.e., in the cortex and the dorsal diencephalon (Fig. 4L,P).

Of note, *Axin2,* which is another transcriptional target of the canonical WNT pathway (Jho et al., 2002), did not show a substantial difference in expression levels between EMM and SOM in the RNAseq data (FC of EMM/SOM = 1.2). RT-qPCR confirmed this result (Fig. S3), and RNA in situ hybridization also showed considerable expression of *Axin2* in EMM (Fig. S8M,P). Since there is functional evidence for active canonical WNT signaling in the apical mesenchyme (Choe et al., 2014; DiNuoscio and Atit, 2019), *Axin2* appears to reflect the activity of this pathway more accurately than *Lef1* or *Myc* in the cranial mesenchyme.

2.3.3. Cell adhesion

Cell adhesion molecules play important roles in many processes of development including tissue patterning, cell differentiation, and cell migration. They not only provide structural support for the tissue, but also modulate signaling pathways (Hynes, 2009; Thiery, 2003).

As mentioned above, laminins are a major component of the basement membrane. (Fig. S5). *Lamc3* (laminin gamma 3) and *Lama1* (laminin alpha 1) were identified to be EMM^{High} by RNAseq (Fig. 5A), but RNA in situ hybridization showed that they were expressed in the meningeal layers of both EMM and SOM (Fig. 5B–G; Figs. S9A–F). Therefore, their enrichment in EMM transcriptome appears to be due to the difference in organization of the tissue, that the meningeal layer has a larger representation in EMM than in SOM. *Sned1* (sushi, nidogen and EGF-like domains 1) mutation in mice caused malformation of craniofacial skeleton (Naba et al., 2018), and an earlier study reported *Sned1* expression in the cranial mesenchyme (Leimeister et al., 2004). We found that *Sned1* was mostly in the meningeal layer (Fig. 5H–J, Figs. S9G–I).

Both *Sorbs1* (sorbin and SH3 domain containing 1) and *Pcdh7* (protocadherin 7) were broadly expressed in EMM, but in SOM, *Sorbs1* was in the meningeal and the chondrogenic layers while *Pcdh7* was in the osteogenic and the dermal layers (Fig. 5K-R, Fig. S9J-O). In the brain, *Sorbs1* was uniformly expressed in both the cortex and the basal ganglia, while *Pcdh7* was expressed in the cortical plate and the basal ganglia mantle zone (Fig. 5K,P). *Wisp1* (WNT1 inducible signaling pathway protein 1, also known as *Ccn4*, cellular communication network factor 4) was predominantly expressed in the outer EMM, and less in the meningeal EMM or SOM (Fig. 5S-U, Figs. S9P–R). *Clec14a* (C-type lectin domain

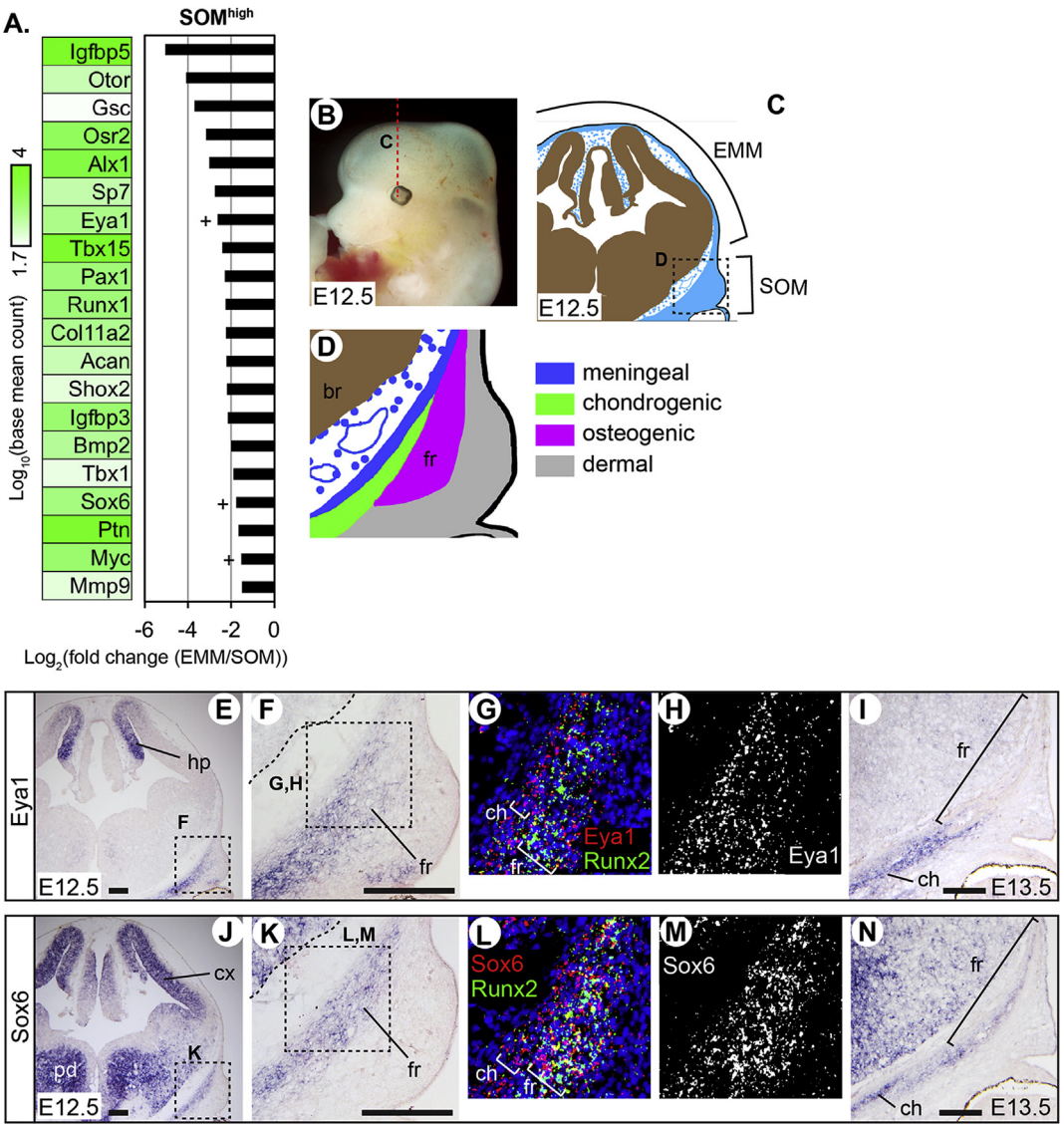

Fig. 3. Skeletal development. A) Genes in the 'skeletal development' category among the top 400 region-specific genes. Expression levels (base mean count) and fold changes from RNAseq are indicated by the color and the bar graphs, respectively. '+' indicates that RT-qPCR test was performed for this gene and it confirmed the differential expression pattern from RNAseq. B) Lateral view of the head of an E12.5 mouse embryo showing the position of the coronal section in C, at the level of the frontal bone rudiment. C) A schematic of the head section with the brain (brown) and the cranial mesenchyme (light blue). D) Four subdivisions of SOM. E-N) Coronal sections of the head at the frontal bone level processed by RNA in situ hybridization. ch: chondrogenic SOM, cx: cortex, fr: frontal bone rudiment, hp: hippocampus, pd: pallidum. Bar, 0.2 mm.

family 14, member a) is a known marker of vascular endothelial cells (Rho et al., 2011). Its expression in the head was limited to these cells, which were more abundant on the apical side (Fig. S9S,T).

2.3.4. *Axon guidance*

Several pathways were represented in this category (Fig. 6A). Semaphorins were first identified as ligands for axon guidance signaling, but subsequently, it has been shown that they also regulate cell migration in broad contexts (Hu and Zhu, 2018; Toledano et al., 2019). In the cranial mesenchyme, *Sema3c* was mainly expressed in the outer EMM but was excluded from SOM (Fig. 6B–F; Figs. S10A–D), which was similar to *Lmx1b* (Fig. S6). In the brain, *Sema3c* was expressed in the lateral pallium of the cortex and the pallidum of the basal ganglia (Fig. 6B). *Ntrk2* (neurotrophic tyrosine kinase, receptor, type 2) was of interest because a mutation in human *NTRK2* was found in a craniosynostosis patient (Miller et al., 2017). *Ntrk2* was expressed in the meningeal layers of EMM and SOM (Fig. 6G–K, Figs. S10E–G). Also, it was strongly expressed in the ventricular zone of the brain (Fig. 6G).

Ephrin-Eph pathway regulates a variety of developmental processes including cell migration and boundary formation (Kania and Klein, 2016). Furthermore, this pathway has been connected to craniosynostosis in humans and mice (see Discussion). Our RNAseq data indicated differential expression of four Eph receptor genes along the apical-basal axis, and we examined two of them in detail. *Epha7* was expressed broadly in EMM, but in SOM it was restricted to the meningeal layer and a small part of the dermal layer (Fig. 6L–P, Fig. S10J-L). In contrast, *Ephb3* was expressed throughout SOM except the meningeal layer (Fig. 6Q–R, Figs. S10H and I). However, by E13.5, *Ephb3* was down-regulated in the osteogenic layer such that neither *Epha7* nor *Ephb3* were expressed in the bone rudiments (Fig. S10T-W). In the brain, *Epha7* was expressed broadly in the cortex and in the diencephalon, while *Ephb3* was mostly in the preoptic area and in the hippocampus (Fig. 6L,Q).

Unc5b (unc-5 netrin receptor B), *Unc5c* (unc-5 netrin receptor C), and *Dcc* (deleted in colorectal carcinoma) encode receptors for netrin family secreted proteins. Although netrin signaling is well-known for regulating axon guidance (Stoeckli, 2018), some studies have suggested its

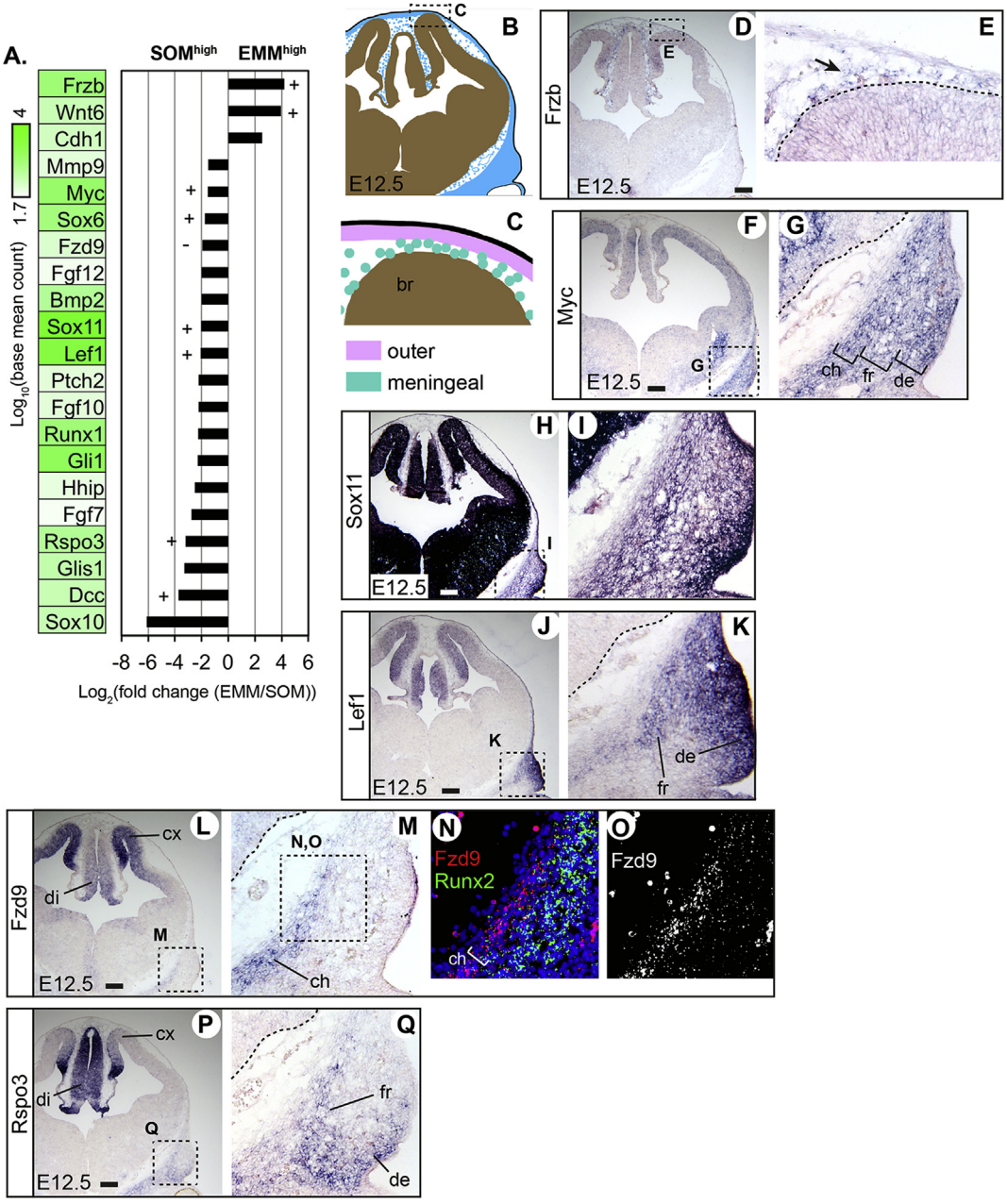

Fig. 4. Cancer pathways. A) Genes in the 'cancer pathways' category among the top 400 region-specific genes. Expression levels (base mean count) and fold changes from RNAseq are indicated by the color and the bar graphs, respectively. '+' and '-' indicate that RT-qPCR test was performed for this gene and it confirmed (+) or did not confirm (−) the differential expression pattern from RNAseq. B) A schematic of the coronal section of the head at the frontal bone level with the brain (br, brown) and the cranial mesenchyme (light blue). C) Two subdivisions of EMM. D-Q) Coronal sections of the head at the frontal bone level processed by RNA in situ hybridization. The arrow in E points to *Frzb* expression in the meningeal EMM. ch: chondrogenic SOM, cx: cortex, de: dermal SOM, di: diencephalon, fr: frontal bone rudiment. Bar, 0.2 mm.

involvement in skeletal development (Hu et al., 2018; Sato et al., 2017). All three netrin receptors were expressed in the cranial mesenchyme, but with distinct patterns. *Unc5b* was expressed in SOM and became specific to the developing calvarial bone by E13.5 (Fig. 6S,T; Fig. S10 M,N,X-c). *Unc5c* was expressed most notably in the chondrogenic SOM but also expressed in some other areas (Fig. 6U–W; Figs. S10O–Q). *Dcc* was only expressed in the dermal SOM (Fig. 6X,Y; Figs. S10R and S). In the brain, *Unc5b* and *Unc5c* were expressed in the dorsal pallium of the cortex and in the diencephalon (Fig. 6S,U). *Dcc* was strongly expressed in the cortical plate of the entire cortex, in the pallidum of the basal ganglia, and in the diencephalon (Fig. 6X).

2.3.5. *Complement and coagulation cascades, innate immune response*

Complement pathway is a part of the innate immune response for clearance of microbes and waste materials from the body (Garred et al., 2016). It also plays an important role during embryonic development such as regulating cell migration and morphogenesis (Leslie and Mayor, 2013). Furthermore, the lectin complement pathway, which is one of the three complement pathways, has been linked to a human birth defect syndrome that includes craniosynostosis (see Discussion). In the lectin complement pathway, pattern recognition molecules such as mannose-binding lectin (MBL) and collectins bind to structures specific to pathogens or damaged cells. This interaction activates MBL-associated

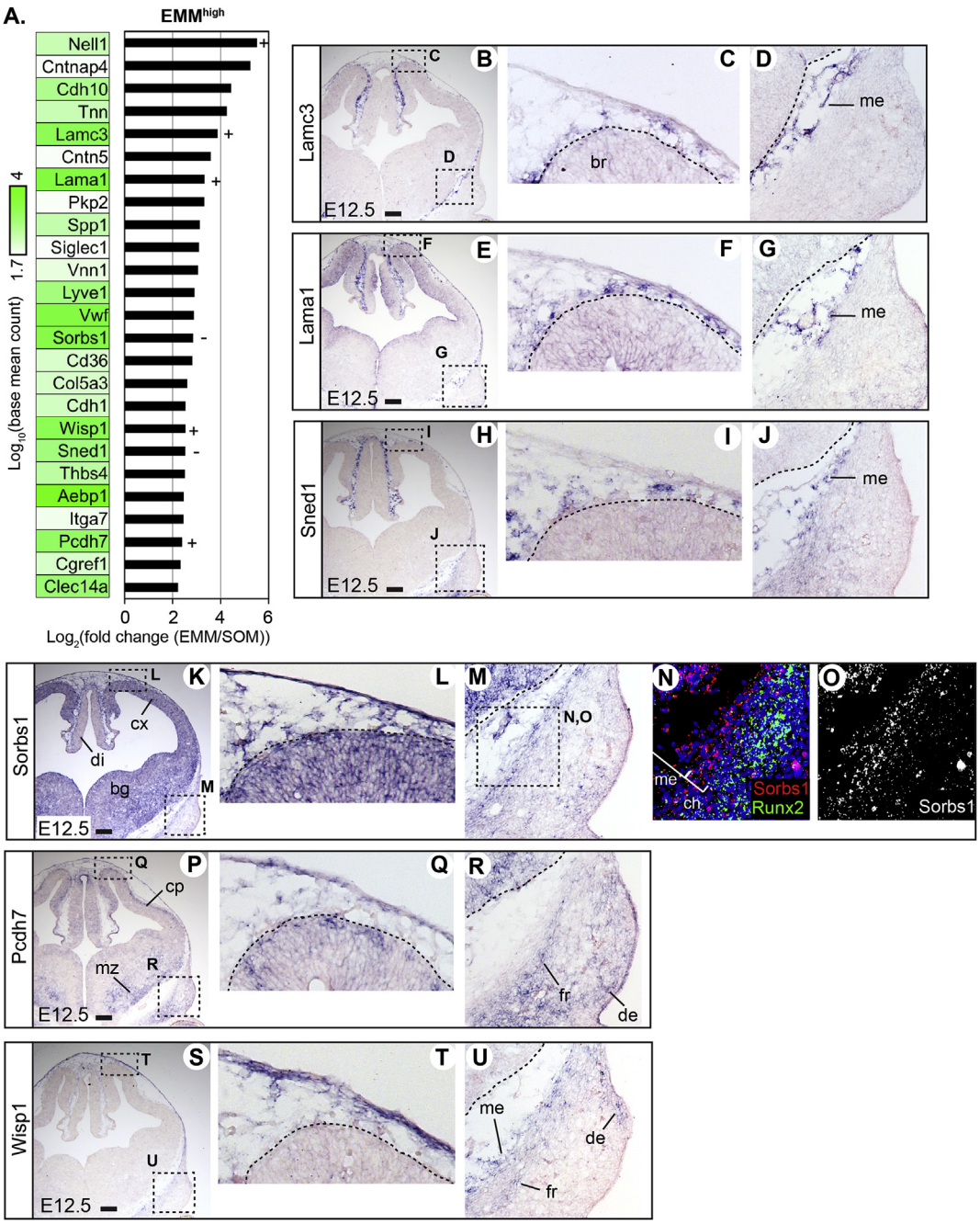

Fig. 5. Cell adhesion. A) Genes in the 'cell adhesion' category among the top 400 region-specific genes. Expression levels (base mean count) and fold changes from RNAseq are indicated by the color and the bar graphs, respectively. '+' and '-' indicate that RT-qPCR test was performed for this gene and it confirmed (+) or did not confirm (−) the differential expression pattern from RNAseq. B–U) Coronal sections of the head at the frontal bone level processed by RNA in situ hybridization. bg: basal ganglia, br: brain, ch: chondrogenic SOM, cp: cortical plate, cx: cortex, de: dermal SOM, di: diencephalon, fr: frontal bone rudiment, me: meningeal SOM, mz: mantle zone. Bar, 0.2 mm.

serine proteases (MASPs), which in turn activate complement components (Dobo et al., 2016; Garred et al., 2016).

Colec12 (collectin sub-family member 12) and *Masp1* were expressed in both layers of EMM (Fig. 7B,C,E,F; Figs. S11A,B,D,E). In SOM, *Colec12* was expressed in the meningeal layer (Fig. 7D; Fig. S11C), and also in the dermal layer at the parietal bone level (Fig. S11C). At the frontal bone level, the outer EMM expression of *Colec12* terminated with a sharp boundary dorsal to SOM (Fig. 7D). Similarly, *Masp1* expression was excluded from SOM at the frontal bone level (Fig. 7G) but extended into the dermal SOM at the parietal bone level (Fig. S11F). *Masp1* was also abundantly expressed in the cortex of the telencephalon (Fig. 7E).

Calca (calcitonin/calcitonin-related polypeptide, alpha) encodes a peptide that is released in response to injury or infection and modulates innate immune responses (Holzmann, 2013). In the head, *Calca* was expressed in EMM at the apex only and in the meningeal SOM near the ventral midline (Fig. 7H–J). We also examined *F13a1* (coagulation factor XIII, A1 subunit) and *Vwf* (Von Willebrand factor), but they were specific to blood cells and the vascular endothelium, respectively, as previously described in other parts of the body (Figs. S11G–J) (Adany and Bardos, 2003; Lip and Blann, 1997).

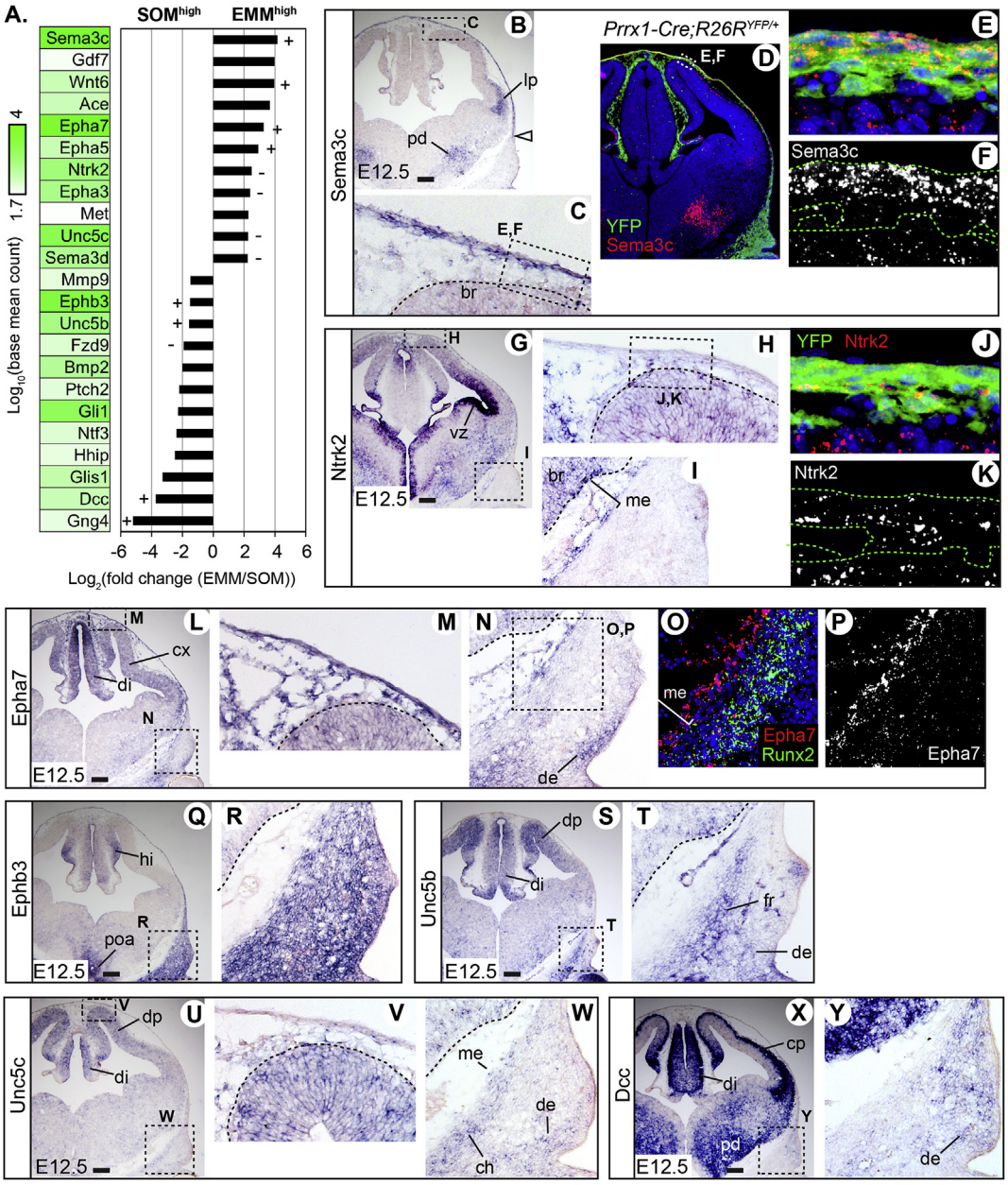

Fig. 6. Axon guidance. A) Genes in the 'axon guidance' category among the top 400 region-specific genes. Expression levels (base mean count) and fold changes from RNAseq are indicated by the color and the bar graphs, respectively. '+' and '-' indicate that RT-qPCR test was performed for this gene and it confirmed (+) or did not confirm (−) the differential expression pattern from RNAseq. B–Y) Coronal sections of the head at the frontal bone level processed by RNA in situ hybridization. D,E, and J also show immunofluorescence for YFP labeling the mesenchyme. The open arrowhead in B points to the ventral limit of *Sema3c* expression. br: brain, ch: chondrogenic SOM, cp: cortical plate, cx: cortex, de: dermal SOM, di: diencephalon, dp: dorsal pallium, fr: frontal bone rudiment, hi: hippocampus, lp: lateral pallium, me: meningeal SOM, pd: pallidum, poa: preoptic area, vz: ventricular zone. Bar, 0.2 mm.

2.3.6. *cAMP signaling*

cAMP (cyclic adenosine monophosphate) is a second messenger that transmits extracellular signals, received by G protein coupled receptors (GPCR), to intracellular effectors such as kinases, transcription factors, and ion channels (Fajardo et al., 2014). The principal function of cAMP is to activate protein kinase A (PKA), which in turn phosphorylates and activates a transcription factor CREB (cAMP response element binding protein) (Wong and Scott, 2004). It is well established that GPCR-cAMP-PKA pathway regulates osteogenesis, and specifically, it was shown to be anti-osteogenic during calvarial development in mice (Xu et al., 2018). Furthermore, reduced cAMP signaling has been associated with craniosynostosis in humans (Graul-Neumann et al., 2009; Salerno et al., 2003).

Adra2a (adrenergic receptor, alpha 2a) encodes a GPCR that is mainly expressed in the central nervous system and responds to hormones (Giovannitti et al., 2015). We found its expression in the meningeal layer of both EMM and SOM, and in parts of the dermal SOM (Fig. 8B–D; Figs. S12A–C). *Adra2a* was also expressed in the striatum of the basal ganglia at this stage (Fig. 8B). *Akap12* (A kinase (PRKA) anchor protein (gravin) 12) encodes a scaffolding protein, and it controls subcellular localization of PKA to facilitate signal transduction (Logue and Scott, 2010; Wong and Scott, 2004). *Akap12* was intensely expressed throughout EMM (Fig. 8E and F; Figs. S12D and E). In SOM, *Akap12* expression was strong only in the meningeal SOM at the frontal bone level (Fig. 8G), and in the meningeal SOM and the dermal SOM at the parietal bone level (Fig. S12F).

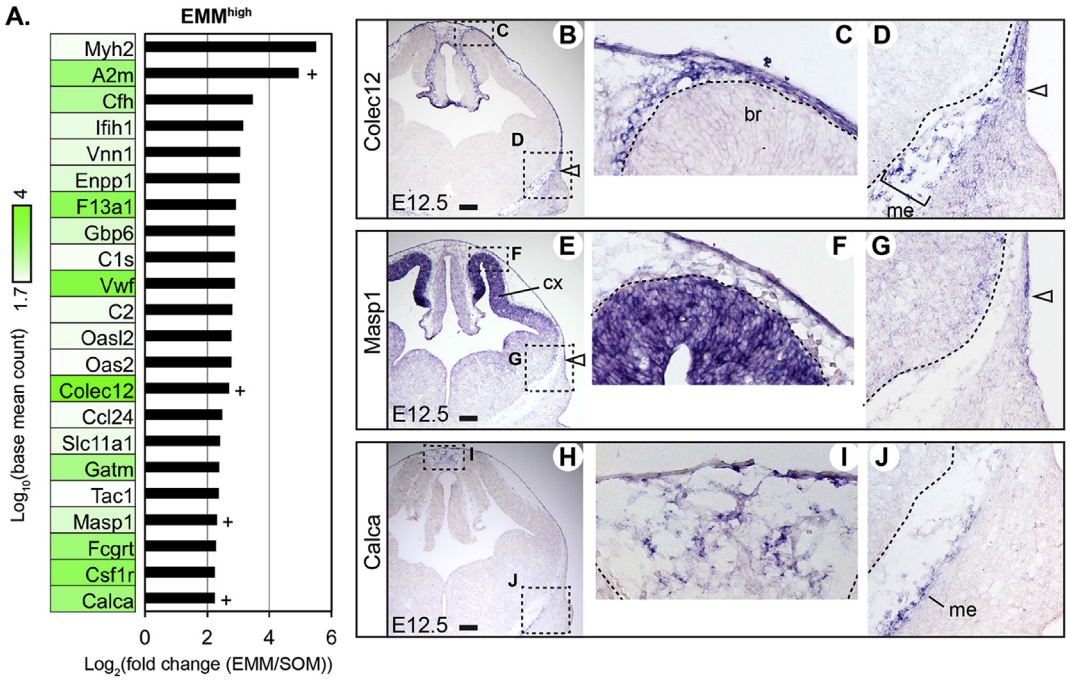

Fig. 7. Complement and coagulation cascade, innate immune response. A) Genes in the 'complement and coagulation cascade' and the 'innate immune response' categories among the top 400 region-specific genes. Expression levels (base mean count) and fold changes from RNAseq are indicated by the color and the bar graphs, respectively. '+' indicates that RT-qPCR test was performed for this gene and it confirmed the differential expression pattern from RNAseq. B-J) Coronal sections of the head at the frontal bone level processed by RNA in situ hybridization. The open arrowheads point to the ventral limits of gene expression continuing from the outer EMM. br: brain, cx: cortex, me: meningeal SOM. Bar, 0.2 mm.

Natriuretic peptide signaling regulates many biological processes including skeletal development (Peake et al., 2014; Santhekadur et al., 2017). NPR3 (natriuretic peptide receptor 3) is a 'clearance receptor' that removes the ligands, but it also modulates cAMP levels (Anand-Srivastava, 2005). NPR3 was shown to decrease or increase cAMP production in different reports (Anand-Srivastava, 2005; Sellitti et al., 2001). In the cranial mesenchyme, *Npr3* showed weak but broad expression in EMM, whereas in SOM it showed very limited expression only in the meningeal and dermal layers (except for the strong perivascular expression) (Fig. 8H–J; Figs. S12G–I). Similar to *Colec12, Masp1*, and *Akap12*, *Npr3* expression in the outer EMM had a sharp ventral boundary at the frontal bone level (Fig. 8J). In the brain, the expression of *Npr3* was limited to the diencephalon roof plate and the choroid plexus (Fig. 8H and I).

Because IPA predicted higher cAMP signaling activity in EMM than in SOM, we examined it using phospho (p)-CREB as a marker. At E12.5, high levels of p-CREB were detected broadly in EMM and in parts of SOM (Fig. 8K-N; Fig. S11J-M). At E13.5, the level of p-CREB remained high in EMM, whereas it was significantly reduced in SOM at the frontal bone level (Fig. 8O–R). This apical-basal difference was not as apparent at the parietal bone level at this stage (Fig. S12N-Q), but it was evident at E15.5 according to a recent report (Xu et al., 2018; see Discussion).

2.3.7. *ZIC transcription factors*

While this category was not identified by GO analyses, we noticed that three genes encoding ZIC (zinc finger protein of the cerebellum) transcription factors, *Zic1, Zic3*, and *Zic4*, were in the list of top 200 EMM^{High} genes. Further examination of the RNAseq data revealed that all 5 members of the mammalian *Zic* family were EMM^{High}, with FC of 2.5–25 and $p < 10^{-7}$ (Fig. 9A). This result was interesting because mutations in human *ZIC1* had been linked to craniosynostosis (see Discussion). *Zic1, Zic3,* and *Zic4* were expressed in both layers of EMM (Fig. 9B,C,G,H,J,K; Figs. S13A,B,D,E,G,H). In SOM, *Zic1* and *Zic3* were expressed in the meningeal layer, and in the dermal layer at the parietal bone level (Fig. 9D,I; Figs. S13C and F). *Zic4* was undetectable in SOM (Fig. 9J; Fig. S13G). Unlike a previous report (Twigg et al., 2015), we did not find *Zic1* expression in the calvarial anlage within SOM, which includes the osteogenic mesenchyme for the frontal bone and the parietal bone, and the prospective coronal suture in between (Fig. 9D,E,F; Fig. S13C).

At E12.5, *Zic1*, *Zic3*, and *Zic4* were all strongly expressed in the diencephalon, but they were expressed in distinct patterns in the telencephalon (Fig. 9B,G,J). *Zic1* was expressed in the hippocampus, cortical hem, choroid plexus, and the pallidum (Fig. 9B). *Zic3* was expressed in all the same areas as *Zic1*, and additionally, in the preoptic area (Fig. 9G). *Zic4* was expressed in the cortical hem, choroid plexus, and the preoptic area, but minimally in the pallidum and not in the hippocampus (Fig. 9J).

Given the direct connection of *Zic1* to human craniosynostosis, we performed a detailed analysis of its expression in the head throughout the second half of gestation. RNAscope technique was used for increased sensitivity. At E10.5 and E11.5, *Zic1* was expressed in the mesenchyme surrounding the brain, but it was already excluded from the mesenchyme above the eye (Fig. 9L–O). Over the following days, *Zic1* was significantly down-regulated in the cranial mesenchyme except in the meningeal layer (Fig. 9P–Z,a; Figs. S13I–V). In particular, *Zic1* expression gradually faded on the lateral side of the head concomitant with the expansion of the calvarial bone into this region, while strong *Zic1* expression was maintained in the mesenchyme of the cranial sutures at the dorsal midline (Fig. 9P–Z,a; Figs. S13I–V). Most of the developing frontal bone was devoid of *Zic1* mRNA (Fig. 9R,S,V,W,Z,a), but some expression was detected at the apical end as the osteogenic front approached the interfrontal suture (Fig. 9Y). Similarly, the parietal bone showed negligible expression of *Zic1* on the basal end (Figs. S13L,R,V), but had some expression on the lateral and apical parts (Fig. S13K,M,N,Q,T,U). Still, the level of *Zic1* expression in the bone was significantly lower than that in the sutures or other surrounding tissues.

3. Discussion

Molecular genetic regulation of cranial mesenchyme patterning remains largely unknown. As the first step of addressing this question, we

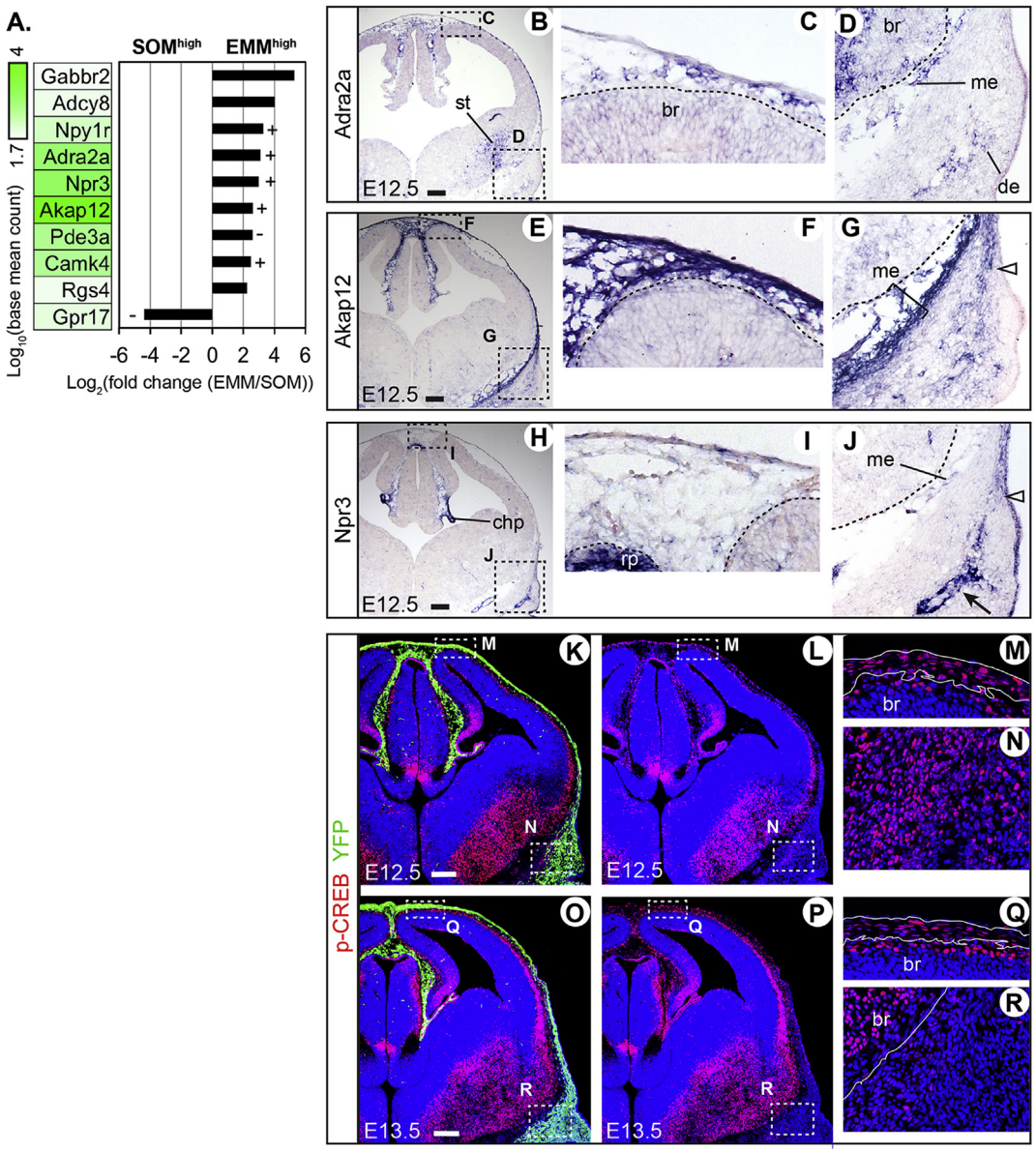

Fig. 8. cAMP signaling. A) Genes in the 'cAMP signaling' category among the top 400 region-specific genes. Expression levels (base mean count) and fold changes from RNAseq are indicated by the color and the bar graphs, respectively. '+' and '-' indicate that RT-qPCR test was performed for this gene and it confirmed (+) or did not confirm (−) the differential expression pattern from RNAseq. B-J) Coronal sections of the head at the frontal bone level processed by RNA in situ hybridization. The open arrowheads point to the ventral limits of gene expression continuing from the outer EMM. K-R) Coronal sections of the head of *Prrx1-Cre;R26R*$^{YFP/+}$ embryos at the frontal bone level processed by immunofluorescence. L and P are the same images as K and O, respectively, without the green channel to better present the distribution of p-CREB around the brain. In M,Q, and R, the white lines demarcate the mesenchyme layer. br: brain, chp: choroid plexus, de: dermal SOM, me: meningeal SOM, rp: roof plate of the diencephalon, st: striatum. Bar, 0.2 mm.

performed a systematic analysis of region-specific gene expression. The information herein can aid future research on development of the cranial mesenchyme in multiple ways. For example, we have documented the expression of almost 40 genes, which provides molecular markers for different areas within the cranial mesenchyme. These markers can be used to assess progression of the regionalization of the mesenchyme during normal development, or to characterize any perturbation in the patterning during abnormal development. In particular, we have identified many genes that are expressed in EMM, where information on gene expression had been scarce. More importantly, the region-specific genes examined here are candidates for novel regulators of cranial mesenchyme development. Many of the genes encode a transcription factor or a component of a signaling pathway. We have focused on the genes preferentially expressed in EMM because this region has received much less attention than the bone-making SOM. However, we have recently reported that *Lmx1b*, expressed in EMM, plays a crucial role in early patterning of the calvaria, which has highlighted the importance of investigating the genetic program of EMM (Cesario et al., 2018).

One of the striking findings of the current work was that a large number of axon guidance genes were expressed in the cranial mesenchyme in distinct patterns. Ephrin-Eph pathway has already been linked to calvarial development because mutations of *EFNA4* (ephrin A4, ligand) and *Epha4* (Eph receptor A4) lead to craniosynostosis in humans and mice, respectively (Merrill et al., 2006; Ting et al., 2009). We found that the components of netrin and semaphorin pathways were also present in the cranial mesenchyme. In particular, *Sema3c* is known to regulate migration of neural crest cells during cardiac outflow tract development (Brown et al., 2001; Feiner et al., 2001; Toyofuku et al.,

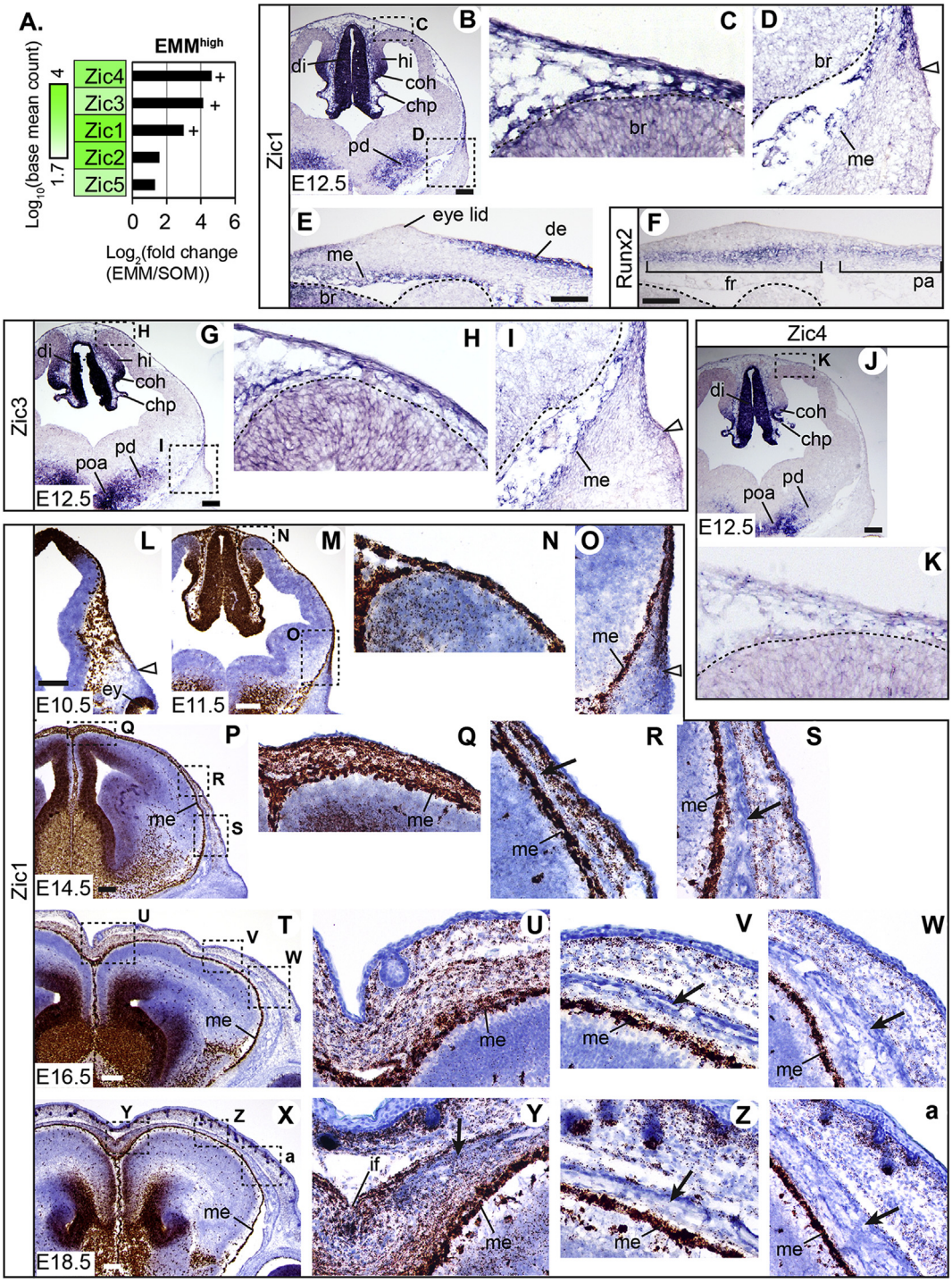

Fig. 9. ZIC transcription factors. A) Genes encoding the 5 members of ZIC transcription factors. Expression levels (base mean count) and fold changes from RNAseq are indicated by the color and the bar graphs, respectively. '+' indicates that RT-qPCR test was performed for this gene and it confirmed the differential expression pattern from RNAseq. B–K) Coronal sections of the head at the frontal bone level (B-D,G-K) or transverse sections of the head through SOM (E,F) processed by conventional RNA in situ hybridization. E and F are adjacent sections. L-Z,a) Coronal sections of the head at the frontal bone level processed by RNAscope in situ hybridization for *Zic1*. The sections were counterstained with hematoxylin. The open arrowheads point to the ventral limits of gene expression continuing from the outer EMM. The arrows point to the developing frontal bone. br: brain, chp: choroid plexus, coh: cortical hem, de: dermal SOM, di: diencephalon, ey: eye, fr: frontal bone rudiment, hi: hippocampus, if: interfrontal suture, pa: parietal bone rudiment, pd: pallidum, poa: preoptic area, me: meningeal layer. Bar, 0.2 mm.

2008), and it was expressed specifically in EMM. Thus, it is an intriguing possibility that SEMA3C might regulate the basal-to-apical migration of osteoprogenitors of the calvarial bone.

This paper is the first to report that lectin complement pathway genes, *Masp1* and *Colec12*, are expressed in the cranial mesenchyme. Mutations in *MASP1*, *COLEC10*, and *COLEC11* have been identified as causes of 3 MC (Mingarelli, Malpuech, Michels, Carnevale) syndrome in humans, which is characterized by facial dysmorphism, cleft palate, craniosynostosis, learning disability, and other developmental defects (Munye et al., 2017; Rooryck et al., 2011; Sirmaci et al., 2010). Based on experiments in zebra fish and in cell/explant culture, it was proposed that COLEC10 and COLEC11 controlled chemo-attraction during initial

emigration of the neural crest cells (Munye et al., 2017; Rooryck et al., 2011). However, we found the expression of *Masp1* and *Colec12* in the cranial mesenchyme at E12.5, which is long after the emigration of the neural crest cells (~E8.5). Therefore, the lectin complement pathway may use an additional mechanism to regulate calvarial development more directly.

We found that cAMP pathway was highly active in EMM at E12.5 and E13.5. cAMP signaling was also active in SOM at E12.5, but down-regulated between E13.5 and E15.5 (our data and Xu et al., 2018). At E15.5, the level of p-CREB was low in the preosteoblasts/osteoblasts of the parietal bone but remained high in the mesenchyme apical to the osteogenic front (Xu et al., 2018). Furthermore, through gain- and loss-of-function experiments in mice, they demonstrated that cAMP signaling was inhibitory to calvarial ossification (Xu et al., 2018). Our data extends their finding in that the high level of cAMP signaling is established on the apical mesenchyme early in calvarial development, and thus it may play a role in the initial patterning.

In addition, our RNA-seq discovered that ZIC family transcription factors were preferentially expressed in EMM. Mutations in *ZIC1* have been linked to both Dandy Walker malformation and craniosynostosis in humans (Grinberg et al., 2004; Twigg et al., 2015). With regard to the function of ZIC1 underlying the craniosynostosis phenotype, it was suggested that *Zic1* was expressed in the calvarial anlage within SOM, and possibly regulated the expression of *En1* here (Twigg et al., 2015). However, we found that *Zic1* was expressed only in the meningeal and dermal layers of SOM, and thus it did not significantly overlap with *En1*. Instead, *Zic1*, *Zic3*, and *Zic4* were co-expressed with *Lmx1b* in the outer EMM at E12.5. As the calvarial development progressed in subsequent stages, *Zic1* expression was gradually reduced and largely excluded from the expanding bone, which further resembled the expression pattern of *Lmx1b* (Cesario et al., 2018). These results suggest that ZIC1 may be an anti-osteogenic factor like LMX1B. More investigation is needed to clarify the role of ZIC transcription factors in calvarial development and craniosynostosis.

While our RNAseq experiment was designed to identify genes expressed in the cranial mesenchyme, many of those examined here were also expressed in the brain. This reflects the fact that common regulatory genes are often used repeatedly in development of different body parts. In addition, for genes making extracellular factors, their expression in the brain can influence the neighboring mesenchyme, and thus the expression in both tissues needs to be considered when investigating the effect on cranial mesenchyme development. Neurosensory organs such as the eye and the ear are another player in skull development, acting through signaling or mechanical interactions (Yang and Ornitz, 2019).

One limitation of the current study is that it provides a very simplified representation of the molecular patterning of the cranial mesenchyme. We have divided the cranial mesenchyme into 6 subdivisions to annotate gene expression, but there is certainly further heterogeneity in the cell population within each subdivision. Capturing the full extent of the complexity of the cells in the cranial mesenchyme would require single cell RNA-seq and computational clustering. When such information becomes available, the in situ gene expression data in this paper can provide zip codes that will allow mapping the various populations of cells onto the actual embryo.

4. Experimental procedures

4.1. Animals

All the animal work in this study was conducted according to protocols and guidelines approved by New York University (NYU) Institutional Animal Care and Use Committee. Wild type C57BL6/J mice were purchased from The Jackson Laboratory (#000664). *Prrx1-Cre* and *R26R*^{YFP} lines were described previously (Logan et al., 2002; Srinivas et al., 2001).

4.2. RNA-seq

EMM and SOM were dissected from wild type C57BL6/J mouse embryos at E12.5 as described in Fig. 1. The embryos were genotyped for y chromosome and only males were used for RNA-seq. We used embryos of the same sex to avoid any sex-related variability in the data, and we chose males because human calvarial defects are more prevalent in males than in females (Michalski et al., 2015). To isolate the mesenchyme, the surface ectoderm and the brain were removed after dispase treatment (3 U/ml, 37 °C for 10 min). 4 samples of EMM and 4 samples of SOM were prepared, where each sample was a pool of tissue from 4 to 5 embryos. The tissue was homogenized using a pestle and QIAshredder (Qiagen), and total RNA was extracted using RNeasy Mini Kit (Qiagen). Subsequent steps of RNA-seq were performed at NYU Genome Technology Center, and the results were processed by NYU Applied Bioinformatics Core. Briefly, cDNA libraries were prepared with poly-A selection using Illumina TruSeq kit. The sequencing was performed by Illumina HiSeq2500 (50 bp single read), which generated 14- to 40-million reads per sample. The reads were mapped to the mouse genome NCBI mm10 by STAR aligner, and the expression levels of genes in each sample were determined using DESeq2 as 'normalized counts' of the reads (Love et al., 2014). DESeq2 was also used for the statistical comparison of gene expression between EMM and SOM. The RNA-seq data have been deposited at Gene Expression Omnibus (accession: GSE128379).

4.3. GO analysis

The lists of top 200 EMM^{High} genes and top 200 SOM^{High} genes were obtained from DESeq2, and submitted to the DAVID website (https://david.ncifcrf.gov/) for functional annotation (Huang et al., 2009). IPA was accessed through a license purchased from QIAgen. For GSEA, the expression data of the whole genome from DESeq2 was uploaded to the website of the program (Subramanian et al., 2005), and it was run for 1000 permutations (type: gene set).

4.4. RT-qPCR

EMM and SOM were dissected from E12.5 wild type C57BL6/J embryos as described previously (Cesario et al., 2018). The ectoderm and the brain were removed manually without the use of dispase. Tissue from 3 to 4 embryos was pooled to make one sample, and the expression of each gene was examined in 4 EMM and 4 SOM samples. Total RNA was extracted as described above, and reverse-transcription was performed using Transcriptor First Strand cDNA Synthesis Kit (Roche). qPCR was performed using Power SYBR Green PCR Master Mix (Applied Biosystems), and a housekeeping gene *Ppib* (peptidylpropyl isomerase) was used as an internal standard (Pachot et al., 2004). mRNA levels of all the genes were normalized against the level of *Ppib* within each sample, using a formula $2(-\Delta Ct(\text{Gene of interest} - Ppib))x1000$. Two-tailed Student's t-test was used to determine whether the expression of a gene was significantly different in EMM and SOM. qPCR primers are listed in Table S8. Most primer sequences are from PrimerBank (Spandidos et al., 2010).

4.5. RNA in situ hybridization

Conventional RNA in situ hybridization and RNAscope in situ hybridization were performed on frozen sections of embryos that were prepared as described before (Cesario et al., 2016). Most sections were from wild type C57BL6/J embryos except for those from *Prrx1-Cre;R26R*$^{YFP/+}$ embryos, which were of mixed background.

Conventional RNA in situ hybridization was performed using probes labeled with digoxigenin or fluorescein as described before (Cesario et al., 2016). The signals were visualized with BM purple alkaline phosphatase substrate (Roche) or TSA Plus kit (PerkinElmer). For most of the anti-sense probes used in this paper, the template was PCR-amplified

from head mesenchyme cDNA of wild type mouse embryos (E12.5-E14.5) or tail genomic DNA of wild type adult mice (for the probes against a single exon). The sequences of the primers for 31 genes are listed in Table S9. All the PCR products were sequenced to confirm the identity. *Lmx1b* probe was described before (Cesario et al., 2018). The probes for *Rspo3* and *Unc5c* were made from commercial plasmids (Rspo3: GenBank accession BC103794, Open Biosystems; Unc5c: GenBank accession BX631000, RZPD). Templates for a few other genes were obtained from other researchers, and the information is available upon request.

RNAscope in situ hybridization was performed using RNAscope 2.5 HD Reagent Kit – BROWN (Advanced Cell Diagnostics, #322300) and the probe for mouse *Zic1* (Advanced Cell Diagnostics, #493121) according to the manufacturer's protocol.

4.6. Immunofluorescence

Immunofluorescence was performed as described before (Jeong and McMahon, 2005). The primary antibodies were chicken anti-green fluorescence protein (Abcam, ab13970, 1:1000), rabbit anti-Laminin (Sigma-Aldrich, L9393, 1:50), mouse anti-SOX9 (Abcam, ab76997, 1:100), rabbit anti-SP7 (Abcam, ab209484, 1:1000), and rabbit anti-p-CREB (Ser133) (Cell Signaling Technology, #9198, 1:500). Alexa Fluorophore-conjugated secondary antibodies (Invitrogen) were used for detection. DAPI (4′,6-diamidino-2-phenylindole) was used to stain the nuclei. Where RNA in situ hybridization and immunofluorescence were combined on the same section, fluorescence in situ hybridization was performed first, followed by immunofluorescence. After binding of the primary antibody, the slides were treated with a peroxidase-conjugated secondary antibody and labeled with Fluorescein-tyramide from TSA Plus kit (PerkinElmer). Fluorescent images were captured with an epi-fluorescence microscope (Nikon Eclipse E600), or a confocal microscope (Zeiss LSM 710) for high magnification pictures.

Conflicts of interest

The authors declare that they have no conflicts of interest with the contents of this article. The content is solely the responsibility of the authors and does not necessarily represent the official views of the National Institutes of Health.

Acknowledgements

We thank Dr. Jean-Pierre Saint-Jeannet and his lab members for sharing the equipment and for helpful discussions. This work was supported by NIH grant R01 DE026798 to JJ.

Appendix A. Supplementary data

Supplementary data to this article can be found online at https://doi.org/10.1016/j.ydbio.2019.07.015.

References

Adany, R., Bardos, H., 2003. Factor XIII subunit A as an intracellular transglutaminase. Cell. Mol. Life Sci. 60, 1049–1060.
Akiyama, H., Lefebvre, V., 2011. Unraveling the transcriptional regulatory machinery in chondrogenesis. J. Bone Miner. Metab. 29, 390–395.
Aldinger, K.A., Lehmann, O.J., Hudgins, L., Chizhikov, V.V., Bassuk, A.G., Ades, L.C., Krantz, I.D., Dobyns, W.B., Millen, K.J., 2009. FOXC1 is required for normal cerebellar development and is a major contributor to chromosome 6p25.3 Dandy-Walker malformation. Nat. Genet. 41, 1037–U1116.
Anand-Srivastava, M.B., 2005. Natriuretic peptide receptor-C signaling and regulation. Peptides 26, 1044–1059.
Angelov, D.N., Vasilev, V.A., 1989. Morphogenesis of rat cranial meninges. A light- and electron-microscopic study. Cell Tissue Res. 257, 207–216.
Bhattaram, P., Penzo-Mendez, A., Kato, K., Bandyopadhyay, K., Gadi, A., Taketo, M.M., Lefebvre, V., 2014. SOXC proteins amplify canonical WNT signaling to secure nonchondrocytic fates in skeletogenesis. J. Cell Biol. 207, 657–671.
Brown, C.B., Feiner, L., Lu, M.M., Li, J., Ma, X., Webber, A.L., Jia, L., Raper, J.A., Epstein, J.A., 2001. PlexinA2 and semaphorin signaling during cardiac neural crest development. Development 128, 3071–3080.
Cesario, J.M., Almaidhan, A.A., Jeong, J., 2016. Expression of forkhead box transcription factor genes Foxp1 and Foxp2 during jaw development. Gene Expr. Patterns 20, 111–119.
Cesario, J.M., Malt, A.L., Chung, J.U., Khairallah, M.P., Dasgupta, K., Asam, K., Deacon, L.J., Choi, V., Almaidhan, A.A., Darwiche, N.A., Kim, J., Johnson, R.L., Jeong, J., 2018. Anti-osteogenic function of a LIM-homeodomain transcription factor LMX1B is essential to early patterning of the calvaria. Dev. Biol. 443, 103–116.
Choe, Y., Zarbalis, K.S., Pleasure, S.J., 2014. Neural crest-derived mesenchymal cells require wnt signaling for their development and drive invagination of the telencephalic midline. PLoS One 9.
Dasgupta, K., Jeong, J., 2019. Developmental Biology of the Meninges. Genesis, e23248.
Day, T.F., Guo, X., Garrett-Beal, L., Yang, Y., 2005. Wnt/beta-catenin signaling in mesenchymal progenitors controls osteoblast and chondrocyte differentiation during vertebrate skeletogenesis. Dev. Cell 8, 739–750.
Deckelbaum, R.A., Holmes, G., Zhao, Z.C., Tong, C.X., Basilico, C., Loomis, C.A., 2012. Regulation of cranial morphogenesis and cell fate at the neural crest-mesoderm boundary by engrailed 1. Development 139, 1346–1358.
Deckelbaum, R.A., Majithia, A., Booker, T., Henderson, J.E., Loomis, C.A., 2006. The homeoprotein engrailed 1 has pleiotropic functions in calvarial intramembranous bone formation and remodeling. Development 133, 63–74.
DiNuoscio, G., Atit, R.P., 2019. Wnt/beta-catenin signaling in the mouse embryonic cranial mesenchyme is required to sustain the emerging differentiated meningeal layers. Genesis 57, e23248.
Dobo, J., Pal, G., Cervenak, L., Gal, P., 2016. The emerging roles of mannose-binding lectin-associated serine proteases (MASPs) in the lectin pathway of complement and beyond. Immunol. Rev. 274, 98–111.
Fajardo, A.M., Piazza, G.A., Tinsley, H.N., 2014. The role of cyclic nucleotide signaling pathways in cancer: targets for prevention and treatment. Cancers 6, 436–458.
Feiner, L., Webber, A.L., Brown, C.B., Lu, M.M., Jia, L., Feinstein, P., Mombaerts, P., Epstein, J.A., Raper, J.A., 2001. Targeted disruption of semaphorin 3C leads to persistent truncus arteriosus and aortic arch interruption. Development 128, 3061–3070.
Ferguson, J.W., Atit, R.P., 2019. A tale of two cities: the genetic mechanisms governing calvarial bone development. Genesis 57, e23248.
Filali, M., Cheng, N., Abbott, D., Leontiev, V., Engelhardt, J.F., 2002. Wnt-3A/beta-catenin signaling induces transcription from the LEF-1 promoter. J. Biol. Chem. 277, 33398–33410.
Garred, P., Genster, N., Pilely, K., Bayarri-Olmos, R., Rosbjerg, A., Ma, Y.J., Skjoedt, M.O., 2016. A journey through the lectin pathway of complement-MBL and beyond. Immunol. Rev. 274, 74–97.
Giovannitti Jr., J.A., Thoms, S.M., Crawford, J.J., 2015. Alpha-2 adrenergic receptor agonists: a review of current clinical applications. Anesth. Prog. 62, 31–39.
Goodnough, L.H., Chang, A.T., Treloar, C., Yang, J., Scacheri, P.C., Atit, R.P., 2012. Twist1 mediates repression of chondrogenesis by beta-catenin to promote cranial bone progenitor specification. Development 139, 4428–4438.
Graul-Neumann, L.M., Bach, A., Albani, M., Ringe, H., Weimann, A., Kress, W., Hiort, O., Bartsch, O., 2009. Boy with pseudohypoparathyroidism type 1a caused by GNAS gene mutation (deltaN377), Crouzon-like craniosynostosis, and severe trauma-induced bleeding. Am. J. Med. Genet. 149A, 1487–1493.
Grinberg, I., Northrup, H., Ardinger, H., Prasad, C., Dobyns, W.B., Millen, K.J., 2004. Heterozygous deletion of the linked genes ZIC1 and ZIC4 is involved in Dandy-Walker malformation. Nat. Genet. 36, 1053–1055.
Han, J., Ishii, M., Bringas Jr., P., Maas, R.L., Maxson Jr., R.E., Chai, Y., 2007. Concerted action of Msx1 and Msx2 in regulating cranial neural crest cell differentiation during frontal bone development. Mech. Dev. 124, 729–745.
Holzmann, B., 2013. Antiinflammatory activities of CGRP modulating innate immune responses in health and disease. Curr. Protein Pept. Sci. 14, 268–274.
Hu, S.H., Zhu, L., 2018. Semaphorins and their receptors: from axonal guidance to atherosclerosis. Front. Physiol. 9.
Hu, X., Liu, Y., Zhang, M., Wang, Y., Lv, L., Zhang, X., Zhang, P., Zhou, Y., 2018. UNC-5 netrin receptor B mediates osteogenic differentiation by modulating bone morphogenetic protein signaling in human adipose-derived stem cells. Biochem. Biophys. Res. Commun. 495, 1167–1174.
Huang, D.W., Sherman, B.T., Lempicki, R.A., 2009. Systematic and integrative analysis of large gene lists using DAVID bioinformatics resources. Nat. Protoc. 4, 44–57.
Hynes, R.O., 2009. The extracellular matrix: not just pretty fibrils. Science 326, 1216–1219.
Ishii, M., Sun, J., Ting, M.C., Maxson, R.E., 2015. The development of the calvarial bones and sutures and the pathophysiology of craniosynostosis. Curr. Top. Dev. Biol. 115, 131–156.
Jeong, J., McMahon, A.P., 2005. Growth and pattern of the mammalian neural tube are governed by partially overlapping feedback activities of the hedgehog antagonists patched 1 and Hhip1. Development 132, 143–154.
Jho, E.H., Zhang, T., Domon, C., Joo, C.K., Freund, J.N., Costantini, F., 2002. Wnt/beta-catenin/Tcf signaling induces the transcription of Axin2, a negative regulator of the signaling pathway. Mol. Cell. Biol. 22, 1172–1183.
Kania, A., Klein, R., 2016. Mechanisms of ephrin-Eph signalling in development, physiology and disease. Nat. Rev. Mol. Cell Biol. 17, 240–256.
Lee, M.H., Kim, Y.J., Yoon, W.J., Kim, J.I., Kim, B.G., Hwang, Y.S., Wozney, J.M., Chi, X.Z., Bae, S.C., Choi, K.Y., Cho, J.Y., Choi, J.Y., Ryoo, H.M., 2005. Dlx5 specifically regulates Runx2 type II expression by binding to homeodomain-response elements in the Runx2 distal promoter. J. Biol. Chem. 280, 35579–35587.

Leimeister, C., Schumacher, N., Diez, H., Gessler, M., 2004. Cloning and expression analysis of the mouse stroma marker Snep encoding a novel nidogen domain protein. Dev. Dynam. 230, 371–377.
Leslie, J.D., Mayor, R., 2013. Complement in animal development: unexpected roles of a highly conserved pathway. Semin. Immunol. 25, 39–46.
Lip, G.Y., Blann, A., 1997. von Willebrand factor: a marker of endothelial dysfunction in vascular disorders? Cardiovasc. Res. 34, 255–265.
Logan, M., Martin, J.F., Nagy, A., Lobe, C., Olson, E.N., Tabin, C.J., 2002. Expression of Cre Recombinase in the developing mouse limb bud driven by a Prxl enhancer. Genesis 33, 77–80.
Logue, J.S., Scott, J.D., 2010. Organizing signal transduction through A-kinase anchoring proteins (AKAPs). FEBS J. 277, 4370–4375.
Love, M.I., Huber, W., Anders, S., 2014. Moderated estimation of fold change and dispersion for RNA-seq data with DESeq2. Genome Biol. 15, 550.
Merrill, A.E., Bochukova, E.G., Brugger, S.M., Ishii, M., Pilz, D.T., Wall, S.A., Lyons, K.M., Wilkie, A.O.M., Maxson, R.E., 2006. Cell mixing at a neural crest-mesoderm boundary and deficient ephrin-Eph signaling in the pathogenesis of craniosynostosis. Hum. Mol. Genet. 15, 1319–1328.
Michalski, A.M., Richardson, S.D., Browne, M.L., Carmichael, S.L., Canfield, M.A., VanZutphen, A.R., Anderka, M.T., Marshall, E.G., Druschel, C.M., 2015. Sex ratios among infants with birth defects, national birth defects prevention study, 1997-2009. Am. J. Med. Genet. 167, 1071–1081.
Miller, K.A., Twigg, S.R., McGowan, S.J., Phipps, J.M., Fenwick, A.L., Johnson, D., Wall, S.A., Noons, P., Rees, K.E., Tidey, E.A., Craft, J., Taylor, J., Taylor, J.C., Goos, J.A., Swagemakers, S.M., Mathijssen, I.M., van der Spek, P.J., Lord, H., Lester, T., Abid, N., Cilliers, D., Hurst, J.A., Morton, J.E., Sweeney, E., Weber, A., Wilson, L.C., Wilkie, A.O., 2017. Diagnostic value of exome and whole genome sequencing in craniosynostosis. J. Med. Genet. 54, 260–268.
Munye, M.M., Diaz-Font, A., Ocaka, L., Henriksen, M.L., Lees, M., Brady, A., Jenkins, D., Morton, J., Hansen, S.W., Bacchelli, C., Beales, P.L., Hernandez-Hernandez, V., 2017. COLEC10 is mutated in 3MC patients and regulates early craniofacial development. PLoS Genet. 13.
Myant, K., Sansom, O.J., 2011. Wnt/Myc interactions in intestinal cancer: partners in crime. Exp. Cell Res. 317, 2725–2731.
Naba, A., Jan, K., Barque, A., Nicholas, C.L., Hynes, R.O., 2018. Knockout of the gene encoding the extracellular matrix protein Sned1 results in craniofacial malformations and early neonatal lethality. bioRxiv 440081.
Novak, A., Dedhar, S., 1999. Signaling through beta-catenin and lef/tcf. Cell. Mol. Life Sci. 56, 523–537.
O'Rahilly, R., Muller, F., 1986. The meninges in human development. J. Neuropathol. Exp. Neurol. 45, 588–608.
Pachot, A., Blond, J.L., Mougin, B., Miossec, P., 2004. Peptidylpropyl isomerase B (PPIB): a suitable reference gene for mRNA quantification in peripheral whole blood. J. Biotechnol. 114, 121–124.
Peake, N.J., Hobbs, A.J., Pingguan-Murphy, B., Salter, D.M., Berenbaum, F., Chowdhury, T.T., 2014. Role of C-type natriuretic peptide signalling in maintaining cartilage and bone function. Osteoarthr. Cartil. 22, 1800–1807.
Rho, S.S., Choi, H.J., Min, J.K., Lee, H.W., Park, H., Park, H., Kim, Y.M., Kwon, Y.G., 2011. Clec14a is specifically expressed in endothelial cells and mediates cell to cell adhesion. Biochem. Biophys. Res. Commun. 404, 103–108.
Rooryck, C., Diaz-Font, A., Osborn, D.P., Chabchoub, E., Hernandez-Hernandez, V., Shamseldin, H., Kenny, J., Waters, A., Jenkins, D., Kaissi, A.A., Leal, G.F., Dallapiccola, B., Carnevale, F., Bitner-Glindzicz, M., Lees, M., Hennekam, R., Stanier, P., Burns, A.J., Peeters, H., Alkuraya, F.S., Beales, P.L., 2011. Mutations in lectin complement pathway genes COLEC11 and MASP1 cause 3MC syndrome. Nat. Genet. 43, 197–203.
Roybal, P.G., Wu, N.L., Sun, J., Ting, M.C., Schafer, C.A., Maxson, R.E., 2010. Inactivation of Msx1 and Msx2 in neural crest reveals an unexpected role in suppressing heterotopic bone formation in the head. Dev. Biol. 343, 28–39.
Salerno, M., Amabile, G., Mandato, C., Di Maio, S., Lecora, M., Avvedimento, E.V., Andria, G., 2003. Growth retardation, developmental delay, distinctive face, multiple endocrine abnormalities, and adenylyl cyclase dysfunction: a new syndrome? Am. J. Med. Genet. 120A, 389–394.
Santhekadur, P.K., Kumar, D.P., Seneshaw, M., Mirshahi, F., Sanyal, A.J., 2017. The multifaceted role of natriuretic peptides in metabolic syndrome. Biomed. Pharmacother. 92, 826–835.
Sato, T., Kokabu, S., Enoki, Y., Hayashi, N., Matsumoto, M., Nakahira, M., Sugasawa, M., Yoda, T., 2017. Functional roles of netrin-1 in osteoblast differentiation. In Vivo 31, 321–328.
Sellitti, D.F., Perrella, G., Doi, S.Q., Curcio, F., 2001. Natriuretic peptides increase cAMP production in human thyrocytes via the natriuretic peptide clearance receptor (NPR-C). Regul. Pept. 97, 103–109.
Siegenthaler, J.A., Pleasure, S.J., 2011. We have got you 'covered': how the meninges control brain development. Curr. Opin. Genet. Dev. 21, 249–255.
Sirmaci, A., Walsh, T., Akay, H., Spiliopoulos, M., Sakalar, Y.B., Hasanefendioglu-Bayrak, A., Duman, D., Farooq, A., King, M.C., Tekin, M., 2010. MASP1 mutations in patients with facial, umbilical, coccygeal, and auditory findings of Carnevale, Malpuech, OSA, and Michels syndromes. Am. J. Hum. Genet. 87, 679–686.
Soriano, P., 1999. Generalized lacZ expression with the ROSA26 Cre reporter strain. Nat. Genet. 21, 70–71.
Spandidos, A., Wang, X., Wang, H., Seed, B., 2010. PrimerBank: a resource of human and mouse PCR primer pairs for gene expression detection and quantification. Nucleic Acids Res. 38, D792–D799.
Srinivas, S., Watanabe, T., Lin, C.S., William, C.M., Tanabe, Y., Jessell, T.M., Costantini, F., 2001. Cre reporter strains produced by targeted insertion of EYFP and ECFP into the ROSA26 locus. BMC Dev. Biol. 1, 4.
Stoeckli, E.T., 2018. Understanding axon guidance: are we nearly there yet? Development 145.
Subramanian, A., Tamayo, P., Mootha, V.K., Mukherjee, S., Ebert, B.L., Gillette, M.A., Paulovich, A., Pomeroy, S.L., Golub, T.R., Lander, E.S., Mesirov, J.P., 2005. Gene set enrichment analysis: a knowledge-based approach for interpreting genome-wide expression profiles. Proc. Natl. Acad. Sci. U. S. A. 102, 15545–15550.
Tagariello, A., Heller, R., Greven, A., Kalscheuer, V.M., Molter, T., Rauch, A., Kress, W., Winterpacht, A., 2006. Balanced translocation in a patient with craniosynostosis disrupts the SOX6 gene and an evolutionarily conserved non-transcribed region. J. Med. Genet. 43, 534–540.
Thiery, J.P., 2003. Cell adhesion in development: a complex signaling network. Curr. Opin. Genet. Dev. 13, 365–371.
Ting, M.C., Wu, N.L., Roybal, P.G., Sun, J.J., Liu, L.Q., Yen, Y.Z., Maxson, R.E., 2009. EphA4 as an effector of Twist1 in the guidance of osteogenic precursor cells during calvarial bone growth and in craniosynostosis. Development 136, 855–864.
Toledano, S., Nir-Zvi, I., Engelman, R., Kessler, O., Neufeld, G., 2019. Class-3 semaphorins and their receptors: potent multifunctional modulators of tumor progression. Int. J. Mol. Sci. 20.
Toyofuku, T., Yoshida, J., Sugimoto, T., Yamamoto, M., Makino, N., Takamatsu, H., Takegahara, N., Suto, F., Hori, M., Fujisawa, H., Kumanogoh, A., Kikutani, H., 2008. Repulsive and attractive semaphorins cooperate to direct the navigation of cardiac neural crest cells. Dev. Biol. 321, 251–262.
Tran, T.H., Jarrell, A., Zentner, G.E., Welsh, A., Brownell, I., Scacheri, P.C., Atit, R., 2010. Role of canonical Wnt signaling/ss-catenin via Dermo1 in cranial dermal cell development. Development 137, 3973–3984.
Twigg, S.R., Forecki, J., Goos, J.A., Richardson, I.C., Hoogeboom, A.J., van den Ouweland, A.M., Swagemakers, S.M., Lequin, M.H., Van Antwerp, D., McGowan, S.J., Westbury, I., Miller, K.A., Wall, S.A., Consortium, W.G.S., van der Spek, P.J., Mathijssen, I.M., Pauws, E., Merzdorf, C.S., Wilkie, A.O., 2015. Gain-of-Function mutations in ZIC1 are associated with coronal craniosynostosis and learning disability. Am. J. Hum. Genet. 97, 378–388.
Twigg, S.R., Wilkie, A.O., 2015. A genetic-pathophysiological framework for craniosynostosis. Am. J. Hum. Genet. 97, 359–377.
Watanabe, M., Kawasaki, K., Kawasaki, M., Portaveetus, T., Oommen, S., Blackburn, J., Nagai, T., Kitamura, A., Nishikawa, A., Kodama, Y., Takagi, R., Maeda, T., Sharpe, P.T., Ohazama, A., 2016. Spatio-temporal expression of Sox genes in murine palatogenesis. Gene Expr. Patterns 21, 111–118.
Wilkie, A.O., Tang, Z., Elanko, N., Walsh, S., Twigg, S.R., Hurst, J.A., Wall, S.A., Chrzanowska, K.H., Maxson Jr., R.E., 2000. Functional haploinsufficiency of the human homeobox gene MSX2 causes defects in skull ossification. Nat. Genet. 24, 387–390.
Wong, W., Scott, J.D., 2004. AKAP signalling complexes: focal points in space and time. Nat. Rev. Mol. Cell Biol. 5, 959–970.
Xu, P.X., Adams, J., Peters, H., Brown, M.C., Heaney, S., Maas, R., 1999. Eya1-deficient mice lack ears and kidneys and show abnormal apoptosis of organ primordia. Nat. Genet. 23, 113–117.
Xu, R., Khan, S.K., Zhou, T., Gao, B., Zhou, Y., Zhou, X., Yang, Y., 2018. Galphas signaling controls intramembranous ossification during cranial bone development by regulating both Hedgehog and Wnt/beta-catenin signaling. Bone Res. 6, 33.
Yang, L.M., Ornitz, D.M., 2019. Sculpting the skull through neurosensory epithelial-mesenchymal signaling. Dev. Dynam. 248, 88–97.
Yoshida, T., Vivatbutsiri, P., Morriss-Kay, G., Saga, Y., Iseki, S., 2008. Cell lineage in mammalian craniofacial mesenchyme. Mech. Dev. 125, 797–808.